School of Electrical and Information Engineering
University of the Witwatersrand, Johannesburg
Private Bag 3, 2050, Johannesburg, South Africa

ELEN4000: Design Project

Antenna Array Design to map man made space "junk" in low earth orbit

October 2018

Submission Date: 23rd October, 2018

Supervisor: Dr. Renier Dreyer

Tristan Kuisis
812587
tristan.kuisis@students.wits.ac.za

ABSTRACT

The increase in space debris over the past few decades has resulted in great difficulty for space agencies and aerospace companies while launching space craft. This space debris poses a risk to this equipment as it is travelling at large relative velocities relative to the craft. The task of this design report is to design and analyse a radar antenna array that is capable of detecting and tracking this space debris which is orbiting the Low Earth Orbit (LEO). This LEO is defined to be 160 km to 2000 km above the Earth's surface and the system is capable of detecting space debris with Radar Cross Sections (RCS) of down to 10 cm in diameter. The system implemented makes use of the monostatic radar configuration and a pulsed wave transmission method in order to detect the space debris and its orbital parameters. The system is made up of an array of 4096 crossed dipole antennas that create a maximum gain of approximately 41.0244 dBi in the main beam which has a Half-Power-Beam-Width (HPBW) of 0.785884° and a side lobe level of 59.639 dB while steering to a maximum of 30° in any direction off of the zenith. This is accomplished with electronic steering by phasing the elements and tapering the power of each element in the array. The system runs on an average of 25.5 kW for the array which equates to a maximum power requirement of 37.83 MW. It operates at a frequency of 610 MHz and has a pulse width of 10 μs which creates a range resolution of 1.5 km. The estimated cost for the system is R 775 million which is within 20 % of similar systems elsewhere in the world. The system is designed to function in the Northern Cape.

Keywords: Monostatic, Bistatic, Antenna, Antenna Array, VSWR, HPBW, Phasing, Space Debris, Crossed Dipole, Pulsed Wave, Continuous Wave, Radar, LEO, Beam Steering, Signal-to-Noise Ratio, Doppler Shift

Contents

List of Figures

List of Tables

1. INTRODUCTION

Over the last six decades, the human race has continuously propelled man made objects into space [1]. These objects have been said to exceed speeds of 66 km/s [2], however, these extremely fast objects often leave the Earth's orbit and travel into outer space. Since the dawn of space exploration, many countries around the world have attempted, and in many cases, successfully deployed man made objects into the Earth's upper atmosphere and into orbits around the Earth.

The organizations running these missions, in the early years, didn't have guidelines on how the missions should be carried out. In addition to this, for many decades, during the Cold War era, countries and organizations took extreme measures to make these missions a success. Many of the missions involved leaving parts of the space craft in the Earth's orbit [3]. Consequently, the number of debris orbiting the Earth grew over the years.

A number of methods are used to deal with this debris (discussed in section C) which have had varying success. An important and efficient method that systems currently make use of is object avoidance. This, however, is coupled with the fact that the location and trajectory of debris in orbit should be known and tracked. This forms the major task of this report. Current solutions can make use of optical sensors (advanced telescopes that visually detect the debris). This system has a major drawback based on the fact that it can only be used during dawn and dusk hours [4–6]. The second implementation makes use of radar techniques. This is the method which is implemented in this system.

This report begins with explaining the background to the task given which includes an explanation of how the radar system works (in principle). This is then followed up with a description of the space debris as well as a number of calculations on the characteristics of this debris. The technology is introduced and optimal frequency is chosen. Once the frequency has been determined, the calculations for the general radar implementation are illustrated. This is followed up by the antenna and array design and simulations. Following that, the feeding network and costing is presented.

1.1 BACKGROUND

Due to the increase in Earth-to-Space launches currently taking place globally, it has become pertinent for space agencies to determine the optimal launch times and characteristics of their missions in order to avoid space debris currently in orbit. This signals the requirement of systems that are capable of detecting this debris from the ground. The aim of the system is such that it is able to detect and track this space debris with the use of phased array radars. A number of assumptions are created in order to carry out the design of this system, these are discussed in the following sections. The idea behind radars is such that an electromagnetic (EM) pulse is created and then launched in a specified direction, this EM wave travels in the specified direction and comes into contact with an object. This object then proceeds to scatter these EM waves in a number of directions. The characteristics of this scattering are discussed in minimal detail in order to characterise the object. The system is then used to receive these scattered EM waves and an assumption is created in order to detect and analyse the signals to identify the object and determine its orbital parameters. It is the design of this system that is undertaken throughout this report.

1.2 Space Debris

The current scope of the project is that it should be capable of tracking space debris that is within the Low Earth Orbit (LEO). This orbit is defined to be approximately 160 km to 2000 km altitude above the Earth's mean sea level. The determination of the orbital parameters of the space debris is calculated in section E1 and E2 as this requires an in depth calculation of the required parameters.

The important parameters acquired from these calculations can be found in table 1.

Table 1: Object Parameters

Parameter	Value	Minimum	Maximum
Object Altitude		160 km	2000 km
Object Slant Distance		184 km	2223.8 km
Object Tangential Velocity		6897.4 m/s	7807.9 m/s
Angular Velocity		0.0034 rad/sec	0.0488 rad/sec
Elevation Angle	60°		
Angle (Measured from Zenith)	30°		
Observable Time		0 s	323.37 s
Apparent Angular Velocity	0.0032 rad/sec		
Linear Velocity		518.14 m/s	6476.8 m/s

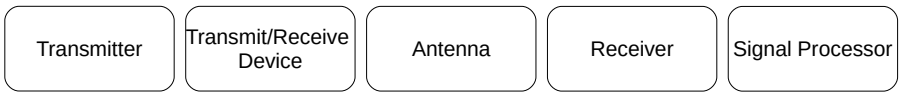

Figure 1: System Overview

1.3 Current Systems

The baseline for this project is built upon the system created by Leo Labs [7]. The Leo Labs system makes use of two systems that are currently installed. These systems form the baseline from which to compare the design of this system. The details of these systems are discussed in section F.

2. TECHNOLOGY

Based on previous implementations of this technology, the best solution is to make use of multiple antennas such that they form an array that can be electronically steered. The basic functionality of the system is that of a radar antenna array where the array sends out a pulse in the form of an EM wave which then bounces off the object and this echo is detected with the use of an array, once this reflection has been received, sampled, and processed, the system is capable of determining a number of characteristics of the object.

The following sections detail the different implementations of this system and determine the advantages and disadvantages of each choice. The system, as an overview is made up of the following components illustrated in Fig. 1 [8].

These components perform the major tasks of the system, they are each discussed in detail in their own sections, however, before that can take place, these components are used to perform a specific action in order to detect the space debris, sections 3., 7., G2, G, and 4.2 introduce the theory behind the operation of this system. The choices for these sections are directly linked to the type of devices and components seen in Fig. 1. The first highly important parameter of the system is the frequency at which it will operate as this is dependent on a number of factors. This is discussed in section 3.

3. OPTIMAL FREQUENCY

A number of constraints exist for the frequency of operation of the system, these range from economical, political, technical, and physical. These constraints and the reasons behind the final choice of frequency are discussed within this section.

3.1 Technical and Physical Limitations

The first limitation of the system is the fact that the ionosphere attenuates frequencies from specific frequency ranges. There are two frequency windows at which EM waves penetrate the ionosphere without excessive attenuation [9]. These frequency windows have a high transmission coefficient for frequencies from the 1 cm to 1 m wavelength range; these frequency bands are highly useful for transmitting EM waves through the Earth's atmosphere as the attenuation is low [10]. Frequencies outside of this window (with a few exceptions to the visible light spectrum), are closed due to ionospheric attenuations and reflections (at larger wavelengths) and also attenuate due to resonances created by molecules in the atmosphere (at lower wavelengths) [10]. If the wavelength of the EM wave is within the bands above, then the attenuation can be considered negligible [11], [8, p. 15,124]. It is apparent that frequencies within this range provide a negligible attenuation of less than 10^{-3} db/km. Based on these assumptions, the optimal frequency band lies within the 200 MHz up to 1 GHz.

The elevation angle of the system is also a contributing factor to the loss of the system as this determines the *volume* of atmosphere that the EM waves travel through to reach the target. Increasing elevation angles result in lower two-way losses, implying that if the system directs its beam directly upwards (towards the zenith), it will have the lowest loss per unit distance [12, p. 70]. This is highly beneficial for the system as it is normally directed upwards and has a FOV that does not greatly increase the *volume* of atmosphere the EM wave has to encounter.

Included in this technical choice is that of currently implemented systems. Many of these operate within the 400 MHz to 500 MHz frequency bands. The amount of electrical power required for these systems can often be in the megawatt range and components capable of supplying this power in the GHz range become prohibitively expensive, this further backs up the choice for a lower frequency.

The frequency that is transmitted from the radar is likely to be different to the frequency that is returned by the object, this is in part due to the Doppler shift phenomenon. The maximum frequency shift created by the Doppler shift is evaluated with the use of equation 1. This implies that the maximum expected Doppler frequency shift is unlikely to exceed $\sim$ 50 kHz based on this equation and the estimates of the maximum linear velocity. This value is created on the assumption that the frequency is 1 GHz which is the upper bound of frequencies that can be selected from.

$$f_d = \pm \frac{2v_r}{\lambda} \tag{1}$$

Where:

- f_d is the frequency shift due to the maximum linear velocity of an object
- v_r is the maximum linear velocity of an object
- λ represents the wavelength of the frequency of choice.

This assumed Doppler shift implies that the frequency bandwidth should accommodate at least 100 kHz on either side of the centre frequency. The Doppler frequency shift of the designed system is discussed in more detail in section 5. where further analysis on the required bandwidth is also analysed as it is dependent on a number of factors.

The frequency choice is highly dependent on the locality of the system and the current frequency usage by other parties as well as population density and frequency usage, which leads to the analysis in section H.

3.2 Characteristics of Frequency

Based on the frequency choice discussed in section H it is clear that the optimal frequency band is the 606 $-$ 614 MHz band; a number of parameters are estimated and illustrated in table 2.

Table 2: Frequency Details

Parameter	Value
Frequency Band	$606 - 614\ MHz$
Centre Frequency	$610\ MHz$
Wavelength	$0.4918\ m$
$\lambda/4$ wavelength	$0.12295\ m$
$\lambda/2$ wavelength	$0.2459\ m$
$3\lambda/4$ wavelength	$0.3689\ m$

The wavelengths generated within this table are based on the centre frequency of the frequency band. This becomes the primary operating frequency of the system.

4. BASIC OPERATION

The first important characteristic of a radar system is the ability to measure the distance of a target from the observation point. This is undertaken with the simple calculation of the amount of time that it takes a signal to travel from the transmitter to the target and back again, this is evaluated with the use of equation 2. This equation evaluates the distance of the target (R) by making use of the speed of light (the speed that the EM wave travels, c), and the amount of time that it took the signal to travel to the target and back again (ΔT).

$$R = \frac{c\Delta T}{2} \tag{2}$$

This allows for the calculation for the maximum and minimum round trip times for specific placements of objects from the observer. Table 3 illustrates the important round trip times which pertain to this system.

Table 3: Radar Range Round Trip Times

Round Trip Time Parameter	Time (ms)
Minimum Distance (Zenith direction)	1.067
Maximum Distance (Zenith direction	13.34
Maximum Slant Distance	14.83

These values take the assumption that the system is capable of steering up to 30° from the zenith direction. If the system were to steer further, then the maximum slant distance would increase accordingly. The maximum steering ability of the system designed is capable of reaching approximately 50°, however, the maximum slant allowed is reduced in order to increase the reliability of the system. This is discussed in more detail in section 7.

Based on the maximum slant distance round trip time ($14.83\ ms$), this places a number of limitations on the system which relate to the pulse repetition frequency, the minimum distance round trip time ($1.067\ ms$), limits the pulse width that the system can transmit over. This also creates a limit on the bandwidth of the system as the bandwidth is related to this parameter by $B = 1/\tau$. The next step in the evaluation of the power that is required to be transmitted onto the object in order to reliably detect it. This begins with the radar range equation.

4.1 Power Density

The power density defines the magnitude of the EM wave as it is returned from the target and is detailed with equation 3, the derivation of this can be found in section I.

$$P_r = \frac{P_t G_t G_r \lambda^2 \sigma}{(4\pi)^3 R^4} \tag{3}$$

Where:

- P_r is the received power at the system
- A_e is the effective aperture of the system
- λ is the wavelength of the system
- G_r is the gain of the receive antenna

4.2 Pulsing Characteristics

In order to calculate a number of characteristics on the Signal-to-Noise ratio (SNR) of the system, the pulsing characteristics are required. Fig. 2a illustrates the method in which the EM waves are sent out with respect to time.

(a) Radar EM Wave Pulse

(b) Object Detection

Figure 2: Radar Functions

The characteristics illustrated in Fig. 2a can be found in table 3 (the explanations are in section 4.). This implies that the maximum pulse width must be less than 1.067 ms, a pragmatic approach would take a value less than this to increase the resolution of the system. The next parameter is the pulse repetition interval, this is related to the maximum round trip time that a signal can take, which implies that the minimum pulse repetition interval should be greater than 14.83 ms. This limits the pulse repetition frequency of the system which is defined as $PRF = 1/PRI = 67\ Hz$. This is the maximum frequency the system can sustain without limiting the radar range abilities.

Fig. 2b represents a case where a pulse is sent outwards and is then followed by, a period of time later, a corresponding echo pulse. The period between the pulse and the echo can be used to determine the altitude that the object has. This illustrates a circumstance of the system detecting an object. In order to detect the pulse, the time between each sample (sampling by the ADC) should be no less than the pulse width of the transmitter, this is a minimum requirement for the sampling frequency of the receiver subsystem.

There are cases where large objects, further out than the maximum slant distance will return a signal (the large RCS results in a larger reflection of EM energy), this signal will be returned after the next pulse has occurred and depending on how far the away the object is, the system can read this as an object that appears to be closer than the actual object. This results in an incorrect reading. These cases should be accounted for within the system such that they are kept to a minimum. In most cases this is not an issue as the object is required to be much larger in RCS for it to be detected. More cases are ruled out as these echoes will appear at the antenna while the second pulse is still being

transmitted, which implies that the receiver is still disconnected. This phenomenon is known as range ambiguity [8, p. 22]

4.3 Resolution

The resolution of the system is made up of three major parameters: range, angle, or/and Doppler frequency. These three parameters highlight the ability for the system to make a distinction between two objects with differing parameters. The first of these, the range resolution, is the parameter which defines the ability of the system to make an effective distinction between two targets that are placed differing distances away from the observation point. It is related to the pulse width of the system as illustrated via equation 4. In order to decide on the pulse width required for the system to function, the criteria for the resolution of the range is required.

$$\Delta R = \frac{c\tau}{2} \tag{4}$$

The limits on the range resolution are coupled with the limits of the bandwidth allowed by the frequency band. The bandwidth allocated to the frequency band is set at 8 MHz, which results in a minimum pulse width of approximately 0.125 μs, which is relatively small when compared to alternative systems [5, 13–18]. The bandwidth required by the maximum Doppler frequency shift of 50 kHz, results in a pulse width of 2 μs. Lastly, the next parameter which determines the magnitude of the pulse width is the fact that the pulse width cannot be larger than the minimum round trip time (as discussed above) of 1.067 ms. This means that the pulse width can be within a 0.125 $\mu s - 1.067$ ms time span. These limits provide a range resolution of 18.75 m and 160.1 km. Increasing the pulse length will result in a higher SNR, however, then the range resolution suffers. Based on this evidence, and current implementations of the system, the pulse width of the system is chosen to be 10 μs. This provides enough time for the transmitter to deactivate, and the receiver to activate to listen to the targets echoes, this switching time is required for the system to perform safely, and to avoid the receiver becoming damaged by the transmitters high power. This pulse width results in a range resolution of 1.5 km, which is sufficient considering the number of objects in LEO and the volume that those objects are within. This distance is 0.075 % of the maximum range of the system. The probability of the system detecting two objects within this ambiguous range are unlikely and therefore this is a sufficient assumption.

This pulse width results in a duty cycle which is evaluated with the use of $DutyCycle = \tau \cdot PRF$, which provides a duty cycle of $675 \cdot 10^{-6}$, this is a relatively small duty cycle, implying that the system is using a small amount of energy with respect to its maximum power requirements. The system constructed should be capable of varying its bandwidth on demand, this provides the ability for the system to scale. The limits on the pulse width are still present for the detection of space debris, however, this technique can be used to detect smaller debris at farther distances. The pulse width is linked to the SNR of the system through equation 5.

$$SNR = \frac{P_t G_t G_r \lambda^2 \sigma}{(4\pi)^3 R^4 k T_s} \tag{5}$$

This implies that an increase in pulse width results in an increase in SNR. This is the case based on the fact that the receiver bandwidth is linked to the waveforms bandwidth, this implies that the receivers bandwidth can be substituted for the pulse width in the standard radar range equation [8, p. 776]. This is a simple method in which to increase the SNR without increasing the cost of the overall system.

5. SNR

The SNR required for this system is highly dependent on the requirements for the probabilities of detection and false alarm. The first simplifying assumption of this section is to assume that the signal received by the object is non-fluctuating, this results in the ability to determine an operational SNR for successful detection [8, p. 102-103]. The derivation for this is found in section J which illustrates the process to define a minimum SNR for successful detection. Based on these calculations, the minimum SNR required is 10 dB.

5.1 Multiple Pulses

The SNR of the system can be improved with the utilization of multiple pulses while the beam is in a certain position. This implies that, if an object enters the field of view of the main beam, based on the HPBW of the system, it will be within the view of the pulse without steering required. These multiple pulses can be averaged in order to increase the performance of the detection [8, p. 66]. This implies that the system can emit multiple pulses, where each pulse increases the SNR achieved for a fixed angular position. The increase in SNR is illustrated in the implementation into the RRE as it has a direct affect on the SNR, this is shown in equation 6.

$$SNR_c(N) = \frac{P_t G_t G_r \lambda^2 \sigma n_p}{(4pi)^3 R^4 k T_0 F B} \tag{6}$$

The value of n_p represents the number of pulses. The minimum number of pulses possible by this system can be determined with the use of equation 17 by using the minimum distance an object can be detected (as this is the minimum amount of time an object will be within the HPBW). This estimate results in a time of 0.5622 s. This implies that, based on the PRI of 14.83 ms, the maximum number of pulses that can be used will be less than 37 pulses. In order to account for *dead time*, a pragmatic value for this can be estimated to be 30 pulses. This effect is incorporated in equations 8 and 9.

5.2 Receiver Noise

The three major losses within any system is made up of the transmitter, receiver, and signal-processing losses. Of these, the receivers' noise is mostly made up of the noise generated by the primary Low Noise Amplifier (LNA) or mixer (if present) [8, p. 405]. This receiver noise is generated by the phenomenon known as thermal noise, this is discussed in section 5.3.

5.3 Thermal Noise

The noise from the environment is mostly made up by solar effects. This case deals specifically with the noise generated by the sun. This can contribute to large amounts of noise within the signal if the antenna array is pointed in the direction of the sun, however, great care should be taken to avoid pointing the antenna array directly at the sun. There will still be a small contribution of the suns noise from the sidelobes of the antenna array, however, this power is greatly reduced. The second source of noise, the largest component within the system, is that generated by the receiver electronics. Thermal noise power, being uniform over the frequency spectrum contributes to the noise power over the bandwidth of the system. This implies that the thermal noise power is directly proportional to the receivers bandwidth. This power is determined with the use of equation 7.

$$P_n = kT_sB = kT_0FB \tag{7}$$

Where:

- k is Boltzmann's constant ($1.38 \cdot 10^{-23} Watt - sec/K$)
- T_0 is the standard temperature (normally 290 K)

- T_s is the system noise temperature ($T_s = T_0F$)
- B is the receivers bandwidth (Hz)
- F is the noise figure of the receiver subsystem.

The noise figure defined here should be given in real amplitude (convert from dB as this is what it is defined as). The bandwidth defined here is a calculated value and is dependent on two factors of the system. Typical noise figures for LNA's range from $2.5 - 5\ dB$, the value used for this calculation is taken to be $2.5\ dB$.

Equation 7 is incorporated into the RRE and is illustrated in equation 8.

$$SNR = \frac{P_t G_t G_r \lambda^2 \sigma n_p}{(4pi)^3 R^4 k T_0 F B} \tag{8}$$

Rearranging this equation and placing the known value on the right hand side results in equation 9.

$$P_t G_t G_r = \frac{SNR_{min}(4\pi)^3 R^4 k T_0 F B}{\lambda^2 \sigma n_p} \tag{9}$$

Where the values on the right hand side of the equation are listed in table 4. This implies that the product of the variables on the left hand side of the equation are required to be equal to the value on the right hand side for the system to function as designed.

Table 4: Major Design Features

Parameter	Value
SNR_{min}	10 dB
R	2223.8 km
F	2.5 dB
B	100 kHz
λ	0.4918
σ	0.0079 m^2
n_p	30
Maximum Doppler Shift	26.338 kHz
Maximum Power	37.8 MW
Average Power	25.5 kW
Duty Cycle	0.00067 %
Maximum Power Per Element	9.235 kW
Average Power Per Element	6.230 W
Pulse Width	10 μs
Range Resolution	1.5 km

The values illustrated in table 4 imply that the entire system is currently designed, the values for the array gain and power are given here in order to illustrate the general operating of the system as the array gains have been calculated in section 7.

6. ANTENNA

The antenna forms the most basic unit of the system. It is responsible for transforming an electrical signal into an EM wave and directing that EM energy into a specific direction. It is also important as it makes use of its reciprocity such that it can receive and transmit with the same characteristics. This makes it ideally suited to this application as it can be used to transmit the EM wave and receive the wave, thus reducing the cost and complexity of the system. The antenna, and corresponding array is designed here to satisfy the requirements in equation 9, these parameters are the systems gain and the power that the system is required to sustain.

The most important design requirement of the antenna is that is should have sufficient gain, it should be able to direct its energy in a specific direction. The second component of the antenna is that it should be capable of sending out this EM wave and receive the echo with minimal losses throughout. The array, discussed in section 7. discusses the design of multiple antennas and their interconnectedness such that the system can benefit from multiple antennas working together. The first design decision is that of the type of antenna to make use of. The design methodology for this has the following criteria: cost, construction, bandwidth, sidelobes, gain, efficiency, power capabilities, durability, polarization (and the Axial Ratio), VSWR, etc. These parameters of the antenna are discussed below and the design is drawn up based on these criteria.

An important consideration for the design process for the antenna is to determine a simplistic antenna that allows for easy construction while also providing the required EM wave characteristics. An important characteristic of the system to consider is to analyse the polarization of EM waves as they progress through the ionosphere and how they are affected by the reflection off of the target. The choice of antenna is a crossed-dipole antenna, the following sections are used to illustrate the process used to determine the correct antenna and how its characteristics were designed and calculated.

6.1 Polarization

There are four commonly used polarizations that are used in antennas: vertical, horizontal, right hand circular, and left hand circular, these are created based on the geometry of the antenna and how it is fed. EM waves entering the ionosphere experience Faraday Rotation, this implies that in the case that a linearly polarized wave passes through the ionosphere, its polarization is rotated from the interaction with the Earth's magnetic field. This interaction is highly dependent on the frequency of the signal and a number of other factors [19, p. 24], which implies that the rotation of this linear EM wave can rotate through an arbitrary amount of degrees based on the environmental conditions at the time of transmission. This rotation implies that if a linearly polarized antenna was used, the receiving antenna would be unable to determine how much the reflected wave had rotated and if it cannot match the exact rotation, then this will result in a significant loss of signal (often up to 20 dB), which can severely impair the system functionality. In order to overcome this, circular/elliptical polarization can be employed as this is not affected in the same way. When using circular polarization, the handedness of the polarization swaps. This implies that if left hand polarization is used on the transmitting antenna, when the EM wave reflects off of the target, the polarization swaps to right hand circular. This results in the requirement for the antenna to be circularly/elliptically polarized, and to have the ability to detect both left and right handed polarization with equal gain magnitudes. Circularly polarized antennas are used for Earth-to-Space and Space-to-Earth communication because of these effects on the polarization. On top of the circularly polarized EM wave, RHCP is commonly used for transmission [20, p. 31].

6.2 Resonant Frequency and Bandwidth

The antenna is designed such that it resonates at the desired frequency (610 MHz), which results in the capacitive and inductive effects cancelling each other out, this makes the antenna efficient. During construction of the antenna, there may be inconsistencies with some of the lengths, so tuning of individual antennas may be required such that they function optimally. In order to counteract this, the antenna is constructed such that it is capable of operating over a relatively wide bandwidth. This bandwidth is specified in section 5.

6.3 VSWR and Return Loss

The antenna is designed to have a maximum VSWR of $1.3:1$ which is sufficient for this application as this represents a return loss of -17.7 dB and lines up with commonly available antennas of similar characteristics [21–24]. The explanation and derivation for these values and decisions can be found in

section K

6.4 Axial Ratio

The axial ratio defines the shape of the ellipse of the EM wave, the aim is to generate an axial ratio which approaches 0 dB, and this value should be chosen such that its magnitude is greater than one to create the RHCP [20, p. 32]. The important procedure to note here is that the polarization is created with the use of creating a phase delay between the two dipoles of the antenna, this delay is set to 90°, this phase shift creates the required polarization and axial ratio.

6.5 Antenna Construction

The physical construction of the antenna is created such that it consists of two half-wavelength dipoles that are aligned at right angles with respect to each other. The currents within these two dipoles have equal magnitude and they are phased 90° apart. Commonly, these crossed-dipole antennas are set up with a reflector such that half of the radiation pattern is reflected in order to double the gain of the antenna [25, p. 108]. Fig. 3a illustrates the geometry of a crossed dipole antenna. The arms of

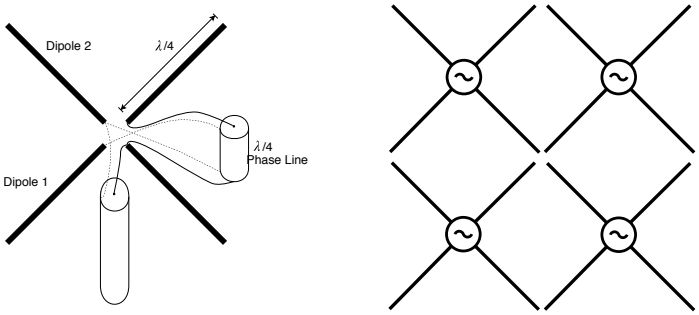

(a) Crossed-Dipole Geometry (b) Array Geometry

Figure 3: Antenna Construction and Array Layout

the antenna illustrated here are positioned parallel to the ground. This is done to create circularly polarized EM waves in the $\pm z$ directions. Clearly, based on the requirements of this antenna, the radiation in the $-z$ direction is not required. The implementation of a perfect electrical conductor placed below the antenna will redirect this part of the radiation pattern upwards where it constructively interferes with the radiation pattern in the $+z$ direction [25, p. 110-111]. This ground plane is required to be placed a quarter wavelength above the ground for this mechanism to work. This mechanism is based on image theory such that the system experiences a doubling in gain [25, p. 111]. This structure is created in FEKO [26] and simulated for the selected frequency. The polar plot and cartesian plots for the radiation patterns are illustrated in Fig. A5 and A6 which can be found in section L. It is important to note from these plots that the antenna which makes use of the ground plane has 3 dB more than the antenna in free space. This implies that the use of a ground plane will increase the performance of each individual antenna without any loss to the ability of the system. The left and right hand circular polarization are not affected by the use of the ground plane either. Based on these simulations a number of characteristics of the two antenna configurations can be compared. This is illustrated in table 7 which is found in section L.

Based on the features in table 7, it is clear that this gain should be multiplied by a large factor in order to meet the requirements stated in section 5.3. This is accomplished with the use of an antenna array, this is discussed in section 7. The antenna geometry is highly important as it should be able to withstand a range of environmental conditions that range from extreme temperatures to humidity variations, to high wind speeds. The ideal material for construction of the antenna is copper as this has the lowest resistivity while having a low cost. The first important parameter of each of the dipoles is to determine the current density throughout the conductor and therefore to optimize the sizing of

the wire such that it takes into account the skin effect. This is calculated with the use of equation 10.

$$\delta = \sqrt{\frac{\rho}{\pi \cdot f \cdot \mu}} = 2.6397 \cdot 10^{-6} m \tag{10}$$

Where ρ is the resistivity of copper ($1.678 \cdot 10^{-8} \Omega m$) and μ is the absolute magnetic permeability of the material ($4\pi \cdot 10^{-7} H/m \cdot 0.999991$). This value for the skin depth implies that the conductor used should, ideally, be a hollow tube which has a wall thickness that should be larger than the size calculated in equation 10. This reduces the cost of each conductor while reducing the weight and therefore the strength of the connectors required. The added benefit of the hollow conductor tube is that it can be expanded to increase the bandwidth of the antenna [27]. The second factor to consider for the thickness of this conductor is related to the power requirements. In order to determine the thickness of this tube, it should be sufficient to dissipate the required amount of power under the maximum temperatures possible in the area. The power that is required to be dissipated by the antenna can be minimized by matching the system, this reduces the losses and hence the power required to be dissipated. The size of this tube should be such that it matches up with the maximum required bandwidth of the system as a whole. The larger the radius of this tube the greater bandwidth the antenna can achieve. The derivation of this sizing is not covered in this report.

7. ANTENNA ARRAY

The antenna array, constructed with multiple individual antennas work collectively in order to augment the radiation pattern. These antennas, in coordination, create a highly directed radiation pattern with higher gain than the individual antennas. The antennas are dynamically phased and excited such that the radiation pattern changes to match the required pattern to detect the debris. The criteria of the array can be satisfied with the correct choice of array factor, element separation, phasing, and the excitation of the individual elements.

7.1 Field of View and Beam Direction

The radiation pattern required, based on the system designed, should be capable of directing the EM wave in the direction of the zenith and be capable of steering 30° away in all directions.

The radiation pattern required from this array should have a large maximum gain with a small beam width. This is required for the system such that it can detect objects in the desired range, while maintaining the cross-range resolution (the ability to make a distinction between two objects within an angle range). This requirement is uniquely suited to the use of a broadside array, in which the maximum radiation is directed in the broadside: $\theta = 0$. In order to accomplish this, the individual antennas maxima should also be in this direction. This justifies the implementation of the crossed dipole. The design of the antenna in the previous section is duplicated for this array, this implies that the sizing of the dipoles, and the height above the ground plane is kept the same ($\lambda/4$). The phase between each dipole keeps the 90° to create the circular polarization.

In order to accomplish this, the antennas are placed in a grid arrangement such that the array forms an $n \times m$ matrix-like shape. The array is then excited such that the main bean is directed towards the zenith. This is accomplished by determining the point at which equation 11 is equal to zero [28, p. 296]. Where Ψ represents the steering angle of the array, $k = \frac{2\pi}{\lambda}$ and β represents the progressive phase delay required between each of the elements.

$$\Psi = kdcos\theta + \beta = 0 \tag{11}$$

This is accomplished by creating a zero phase delay between the elements. This applies to the case of the uniformly excited array, which implies that all elements in the array have the same amplitude excitation. This achieves the zenith direction gain of the array. The next stage is to determine the optimal spacing between each element.

7.2 Element Spacing

The second requirement of this broadside radiation is that there should be no other maxima in the radiation pattern, this phenomenon is known as grating lobes. The presence of side lobes within the radiation pattern is unwanted as this can result in large amounts of radiated energy in unwanted directions. These sidelobes also result in a misuse of the energy for the system. The reduction of side lobe level is discussed in more detail in section 7.5.

The spacing between each element in the array is set at $\lambda/2$ which satisfies this criteria for the technical and practical limitations, and the derivations for this specification can be found in section M.

7.3 Main Beam Gain

The gain of the main beam is highly important to the functionality of the system. This part of the design is created such that the antenna array is sized so that gain is maximized while maintaining a practical number of elements. The design procedure for sizing the array is based on a number of factors. The first of these is based on previous implementations of antenna arrays to detect space debris [13], this made use of an array of 64×64 elements which creates a total of 4096 elements. The second design choice is the fact that this sizing results in the ability to create a modular design with the elements. The sizing of this array is structured such that it is a matrix-like shape, making phasing ability the same for both steering directions and creates a relatively linear steering FOV. During simulations, the increase in gain between a 64×64 matrix and a 70×70 array resulted in an increase of 0.775 dB, which does not warrant the extra cost for the extra 804 antennas. Increasing the number of antennas reduces the power requirement for each antenna as this splits the total power requirement between each antenna, however, the additional cost incurred for each element unit is not feasible. The next stage is to attempt to steer this main beam in the required directions to track the debris. The steering of the system is discussed in section 7.4. To illustrate this feature of the system, Fig. 4 shows the differences between a 32×32, 64×64, and a 70×70 array and the different gains they each produce.

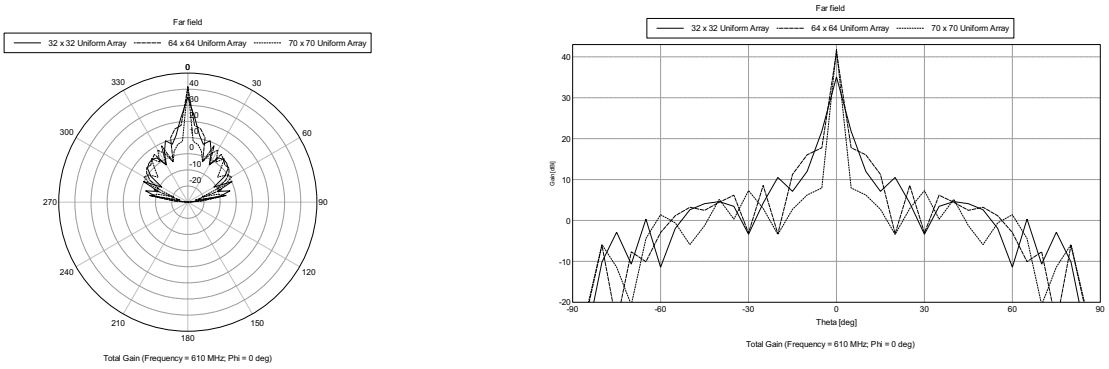

(a) Main Beam Gain for Different Array Sizes - Polar Plot (b) Main Beam Gain for Different Array Sizes - Cartesian Plot

Figure 4: Main Beam Gain for Different Array Sizes

The drawback of increasing the number of elements in the array (even though the main beam gain has increased), is that the side lobe level decreases. This implies that these side lobes may be capable of creating false detections. If the side lobe levels are high enough, they may be capable of sending out an EM wave with enough energy such that the returned pulse is detected as an object. Depending on the direction of these side lobes, it may be low flying aircraft, birds, objects in the low range of LEO, etc. Consequently, these side lobes should be reduced such that they do not affect the system. Side lobes can create unwanted interference between neighbouring systems which is unfavourable for both systems. In the case that the beam is steered in its maximum angle, this side lobe is steered as well. A number of methods exist in which to reduce this effect, the first is to attempt to reduce the side

lobes. The reduction of these side lobes is discussed further in section 7.5.

The ground plane is highly important to the array, just as it was important for the gain in the individual element. The ground plane creates the 3 dB increase when it is present. The simulated illustration can be found in section refsec:GroundPlaneCharacteristics. Table 5 lists the important parameters from the three different arrays in Fig. 4 as these parameters are pertinent to the functioning of the system.

7.4 Element Phasing

In order to achieve steering of the array, progressive phase delay is used for consecutive elements. This phase delay amount is determined with the use of equation 12 [28, p. 301].

$$\Psi = kdcos\theta + \beta \tag{12}$$

In this case Ψ represents the angle to which the array should direct its main lobe, θ is taken to be $0°$ (to create the broadside effect) and β the progressive phase delay for each element. This principle is used to illustrate the scanning feature represented in Fig. A9 and A10 where different scanning angles are illustrated by the differing curves. This scenario makes use of a 32×32 array where the steering is increased by $10°$ increments. This is then scaled up to the standard sized array used for the system, this is illustrated in Fig. 5.

This principle can be applied continuously which means that the beam can be dynamically steered in the required direction. In order to apply this principle to the 2D array used in this design, the steering is implemented in the x direction, and then the y direction, such that the beam is steered in the θ and then the ϕ direction in order to be directed at the required coordinates. This system is analysed with the use of FEKO in order to test the steering ability of the system [26]. The Python code used to generate the phasing can be found in section S. The introduction of more antenna elements results in

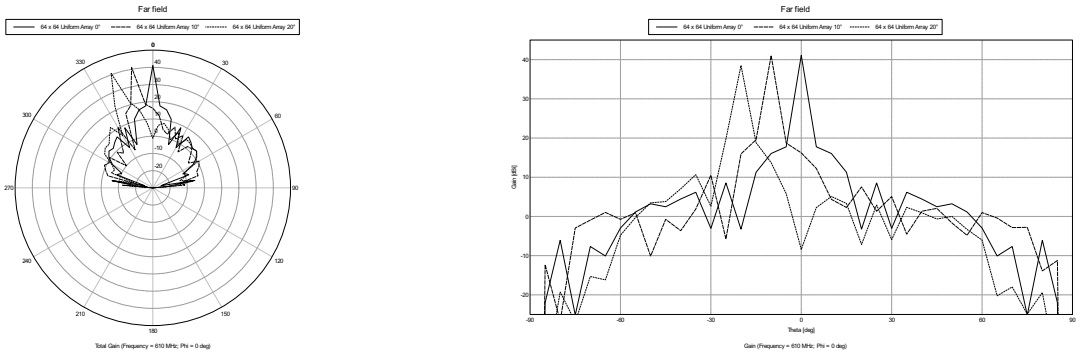

(a) 64×64 Array Beam Steering Ability - Polar Plot (b) 64×64 Array Beam Steering Ability- Cartesian Plot

Figure 5: 64×64 Array Beam Steering Ability

a decreasing main beam width, which increases the cross-range resolution when detecting objects[8, p. 14,28,469]. The phasing is achieved with the feeding network which is designed in section 7.6.

7.5 Element Excitation

Side lobe level of an array is always present in cases where a uniform excitation of the array is used. These side lobes can become dangerous when the size and power level of the array becomes large. There are a number of ways in which to reduce the side lobes: Uniform, Binomial, and Tschebyscheff [28, p. 324-325]. Uniform is the standard case which has been used up to this point, and the Tschebyscheff is not implemented in this system. The uniform distribution does not attempt to reduce the side lobes, however, it is simple to implement in many situations as this reduces the cost and complexity

of the system. The second makes use of the Binomial distribution in order to weight the power which excites each antenna element. This method however, implies that in the case that the array becomes large, the outside elements contribute minuscule amounts of power to the system. Consequently, a compromise between the binomial and the uniform amplitude is created. This is done such that, the power is tapered from the centre of the array, and the power is tapered down to a set point at the edges of the array. This tapering is set to be a 50 % value such that the middle elements transmit 100 % of the power, and the outside transmit 50 % of the power. This results in a pyramidal distribution on the array as it tapers off to the edges. This power taper in the elements is illustrated in Fig. 6a where the darker colour represents a higher power. The result of this amplitude excitation is illustrated in

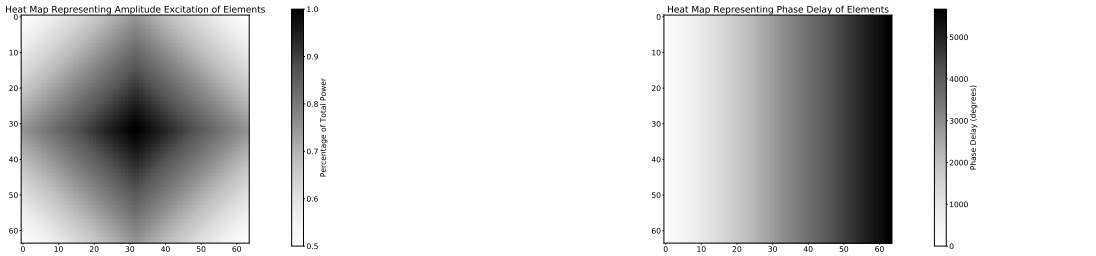

(a) Power Tapering (b) Heat Map Representing the Phase Delay of Each Element

Figure 6: Heat Maps Representing Power Tapering and Phase Delays

Fig. 7 where a uniform 64×64 array is compared with the tapered 64×64 array. It is clear from this illustration that there is a major increase in side lobe level which results in a more efficient and accurate system. This now reduces the chances of the system detecting objects from the side lobes. The decreased HPBW results in a greater cross-range resolution which enhances the capabilities of the system. The result of this tapering is measured and quantified in table 5.

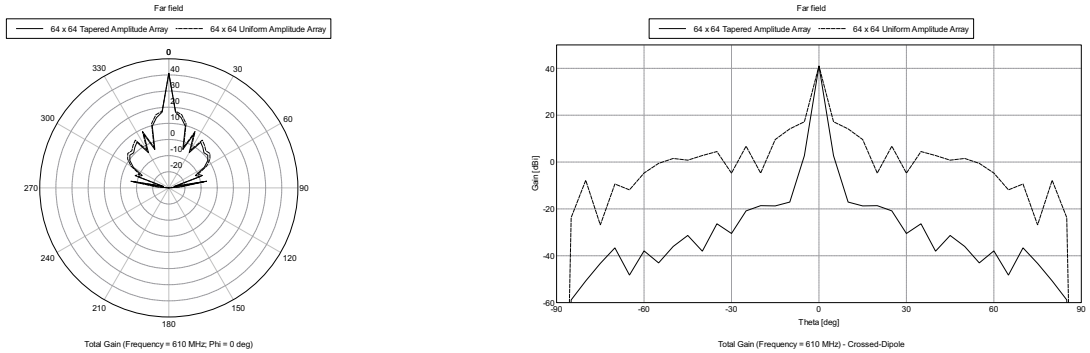

(a) Uniform vs Tapering - Polar (b) Uniform vs Tapering - Cartesian

Figure 7: Amplitude Excitation with Uniform compared to Tapering

Table 5: Amplitude Tapering Details

Parameter	Uniform Array	Tapered Array
Maximum Gain (dBi)	41.1059	41.0244
Side Lobe Level (dB)	32.5337	59.639
Half Power Beam Width (-3 dB)	1.28995	0.785884

7.6 Feeding Networks

In order to reduce the cost of the overall system, each antenna is designed such that it has its own feeding network. This implies that if a part of a feeding network is damaged, then the only replacement

will be for that individual antenna. This makes the system highly modular. The feeding network is designed such that each antenna element communicates with a central command module (CMM). This CMM is responsible for the phasing and amplitude selection for each individual antenna element. The communication between each antenna element is by means of a fibre optic cable. This communications medium reduces the noise on the system as it is not making use of electrical currents which can interfere with the operation of the system. This modular system is created to be similar to the AMISR's implementation [13], which makes use of modular panels such that there are multiple antennas per module, each module has its own controlling unit, and these controlling units communicate with the CMM. This implementation is improved in this design based on the newer technology available which allows for higher modularity of the components and higher data communication throughput. This modular design means that multiple antenna elements can fail with the overall system still functioning sufficiently.

This implementation also results in a simplified feeding mechanism as matching between multiple antennas is no longer required. The implementation of solid state amplifiers is used here as they are highly reliable, easily maintainable, and are modular in nature. The down side of solid state amplifiers is that they are not able to generate large amounts of power [8, p. 364], however, due to the fact that the power is split between each element in the array, they are ideally suited to this application. The implementation of solid state technology results in the use of DC voltages throughout the system, this is an important factor for this implementation as DC creates minimal interference to the antennas. Consequently, the radiating elements are located within the element module and the connector cables from the module to the antenna. The interference from the electronics within the module can be reduced with the use of shielding the walls of the module. The connector cables make use of sleeve baluns which reduce the radiating components commonly seen on coaxial cables. Throughout the system, RoHS parts are required [29], as well as lead free solder for a the construction and assembly of the array elements and control systems. The details for the transmitter and receiver are covered in section Q which illustrates the components required for their construction.

8. COSTING ANALYSIS

The costing analysis for this design takes into consideration a number of similar systems and their implementations of the array. These costings are analysed for the use case in question. The systems designed cost is estimated to be R 775.95 million which is within 20 % of a comparable system. The analysis, array and antenna costing can be found in section R

ACKNOWLEDGEMENT

The author would like to thank Dr. Renier Dreyer for supervising the design project throughout the six week period and for guiding the process of the design. The author would also like to thank Dr. Derek Nitch for the invaluable input for the designing of the system.

9. CONCLUSION

The system designed makes use of standard radar techniques with the use of an antenna array in order to track space junk within the 160 km to 2000 km altitudes which make up the LEO, the system is capable of detecting space junk with a RCS of 10 cm in diameter in this range. The system is built to function with an average of 25.5 kW and a maximum power of 37.83 MW which lie within the ranges of similar systems. The system has the ability to detect and track this space debris any time of day. The system makes use of an array of 4096 crossed dipole antennas in a matrix-like geometry and it is capable of steering its main beam by 30° from the zenith. The cost of the system is estimated to be R 775 million which is within 20 % of similar systems. The system is ideally located in close proximity to the Square Kilometre Array (SKA) installation in the Northern Cape and will operate at a frequency of 610 MHz.

REFERENCES

[1] A. Zak. "First artificial satellite orbits the Earth.", October 2018. URL https://goo.gl/NQZYtn.

[2] W. Gurstelle. "The Nuclear Potato Cannon Part 2.", January 2006. URL https://goo.gl/hGwrJd.

[3] A. S. Academy. "A GUIDE TO ORBITAL SPACE DEBRIS.", 2010. URL https://goo.gl/WpCRRp.

[4] C. on Space Debris. "Orbital Debris - A Technical Assessment." 1995.

[5] J. R. Snell. "Optimizing orbital debris monitoring with optical telescopes." September 2010.

[6] M. A. Earl. "DETERMINING THE ORBIT HEIGHT OF A LOW EARTH ORBITING ARTIFICIAL SATELLITE OBSERVED NEAR THE LOCAL ZENITH." October 2006.

[7] L. LABS. "LEO LABS.", October 2018. URL https://goo.gl/b54skV.

[8] M. Richards, W. Holm, and J. Scheer. *Principles of Modern Radar: Basic Principles*. Electromagnetics and Radar. Institution of Engineering and Technology, 2010. URL https://goo.gl/az8neA.

[9] T. Hasenohr. "Initial Detection and Tracking of Objects in Low Earth Orbit." URL https://goo.gl/WctGfF.

[10] H. Klinkrad. *Space Debris: Models and Risk Analysis*. Springer Praxis Books. Springer Berlin Heidelberg, 2006. URL https://goo.gl/zZtoUj.

[11] I. T. Union. "Attenuation by atmospheric gases.", September 2016. URL https://goo.gl/RKxp8S.

[12] G. Curry. *Radar Essentials: A Concise Handbook for Radar Design and Performance Analysis*. Electromagnetics and Radar. Institution of Engineering and Technology, 2011. URL https://goo.gl/yiHxpz.

[13] T. Valentic, J. Buonocore, M. Cousins, C. Heinselman, J. Jorgensen, J. Kelly, M. Malone, M. Nicolls, and A. V. Eyken. "AMISR the advanced modular incoherent scatter radar." In *2013 IEEE International Symposium on Phased Array Systems and Technology*, pp. 659–663. Oct 2013.

[14] J. Markkanen, M. Lehtinen, and M. Landgraf. "Real-time space debris monitoring with EISCAT." *Advances in Space Research*, vol. 35, no. 7, pp. 1197 – 1209, 2005. URL https://goo.gl/S3q4x3. Space Debris.

[15] D. Agaba, M. Inggs, and D. O'Hagan. "SIMO radar design for small space debris detection in the LEO." In *2015 IEEE Radar Conference (RadarCon)*, pp. 0551–0554. May 2015.

[16] A. Patyuchenko, M. Younis, and G. Krieger. "Reflector-based digital beam-forming radar system for space debris detection." In *11-th INTERNATIONAL RADAR SYMPOSIUM*, pp. 1–4. June 2010.

[17] A. Morselli, P. D. Lizia, G. Bianchi, C. Bortolotti, S. Montebugnoli, G. Naldi, F. Perini, G. Pupillo, M. Roma, M. Schiaffino, A. Mattana, E. Salerno, A. Magro, K. Z. Adami, R. Armellin, A. L. Sergiusti, W. Villadei, F. Dolce, M. Reali, and J. Paoli. "A new high sensitivity radar sensor for space debris detection and accurate orbit determination." In *2015 IEEE Metrology for Aerospace (MetroAeroSpace)*, pp. 562–567. June 2015.

[18] J. G. Trujillo, S. Halté, M. S. Pérez, and P. Besso. "On the design of a planar phased array radar antenna architecture for space debris situational awareness." In *2013 7th European Conference on Antennas and Propagation (EuCAP)*, pp. 254–255. April 2013.

[19] D. Sjoberg. "EITN90 Radar and Remote Sensing: Space-based SAR for remote sensing.", 2018. URL https://goo.gl/Vx1xRP.

[20] M. Katragadda. "Design and Simulation of a Planar Crossed-Dipole Global Navigation Satellite System (GNSS) Antenna in the L1 Frequency Band." December 2012. URL https://goo.gl/4myNJB.

[21] "Base antenna LEO eggbeater 70 cm 430-440 MHz RHCP.", October 2018. URL https://goo.gl/sjtqoS.

[22] "Turnstile crossed dipole NOAA receiving antenna for 137MHZ-139Mhz.", October 2018. URL

https://goo.gl/vsghnE.
[23] "Turnstile crossed dipole antenna for 430 - 440Mhz (70cm).", October 2018. URL https://goo.gl/tJXSuF.
[24] "Turnstile crossed dipole Cubesat receiving antenna for 144Mhz-146Mhz (ISS,APRS,IGATE,SSTV).", October 2018. URL https://goo.gl/ECty3k.
[25] S. X. Ta, I. Park, and R. W. Ziolkowski. "Crossed Dipole Antennas: A review." *IEEE Antennas and Propagation Magazine*, vol. 57, no. 5, pp. 107–122, Oct 2015.
[26] A. Engineering. "Electromagnetic Simulation Software — Altair FEKO.", October 2018. URL https://goo.gl/pXimYF.
[27] A. Theory. "Broadband Dipole Antenna.", October 2018. URL https://goo.gl/au5bsW.
[28] C. Balanis. *Antenna Theory: Analysis and Design*. No. v. 1 in Antenna Theory: Analysis and Design. John Wiley & Sons, 2005. URL https://goo.gl/RnbPim.
[29] RoHS. "RoHS Guide.", OCtober 2018. URL https://goo.gl/ZoiF92.

Appendix

A NON-TECHNICAL REPORT: SOCIAL, ECONOMIC, AND ENVIRONMENTAL IMPLICATIONS

In any engineering design, there are a number of impacts that should be considered throughout the design process. The impacts of any project can be estimated and accounted for ahead of the implementation of the system. These impacts are both beneficial and harmful to the external parts of the system. These are discussed in the following sections.

A1 Social Implications

The implementation of such a system requires a large amount of effort on the part of the local community as well as the government and research institutions. The construction and installation of this system is unlikely to have an immediate effect or be of benefit to the South African community as this system is commonly used by first world countries with large scale space-related projects. Countries such as America, China, and Russia require the use of such systems as they allocate large portions of their spending to space exploration and research, while large private corporations launching satellites will benefit from the system as well. The slowly increasing endeavours by South African National Space Agency (SANSA) will benefit from such a system, however, the justification of such a system primarily for SANSA does not make economical sense [1].

The intended use of this system is to detect space debris, which will primarily benefit the parties stated above, however, the system (based on research of similar such systems [2, 3]) have proved to be of use in the scientific research space. The nature of space debris is that it is unlikely to require tracking the entire time, and as such, other institutions may make use of the system for research purposes. The system, in essence is an EM wave generator that is steerable, this implies that the data that it generates can be analysed and used in a number of alternative applications. This implies that the SKA, currently near the ideal location of this system, would also benefit from the installation of this system.

The nature of such an installation is that it will require large amounts of investment and construction. This implies that for the duration of construction, the local community will benefit as temporary employment will increase. This installation will also require the stationing of a number of permanent staff, these staff will in turn bring in customers, these customers will bring investment and revenue to the local communities and the country as a whole.

Such systems are often boasted to local communities and create large impacts on the STEM professions which benefit the country over time.

Depending on the circumstances of the construction, there may be farm lands which will be affected, the farmers should be compensated for this by abiding to the local laws. The NSF has set up such a system for the SKA and as such, similar guidelines can be employed for the process [4].

This project benefits manned missions into LEO as it improves the safety for launches and long duration stays in LEO.

A number of space debris currently in orbit is radioactive, this is the case as multiple satellites and missions made use of radioisotope thermoelectric generators which have, in some cases, entered Earth's atmosphere and caused damage to areas of land [5]. The tracking of these types of debris is highly important as it provides early warning mechanisms to affected areas.

A2 Economic Implications

The current system design is set to cost approximately R 775 million and will continue to have ongoing costs for the daily operations and maintenance. This system should therefore be beneficial to warrant its implementation. The major customers for this system are likely to be space agencies from first world countries and large commercial organisations which deal in the aerospace industry. Consequently, this system is required to have a strategy in which to recuperate its costs. The system is highly beneficial to the scientific community in addition to these corporate interests, and this addition is challenging to place a value to.

The system will greatly benefit the local towns as it will bring international customers and investors as stated in the above section.

A3 Environmental Implications

The system involves the installation over a large area of land, large energy consumption, and radiation directly into the atmosphere as such these should be analysed to determine how they can possibly affect the surrounding area.

The installation will cover a large area of land, this installation will also require the clearing of the surface of the land. Environmental studies should be undertaken to determine if any local flora/fauna will be affected by the installation. The impact of the system to these organisms should be minimized as much as possible.

The implementation will involve the installation of a water source such that technicians and operators can work on-site. This water requirement will need to be investigated as the local areas do not receive a large amount of rainfall and placing such a burden on the local communities water supplies is not advised. Drilling for boreholes should be the first test, and in the case that the ground water level is too deep, or not present, then the costing of importing water should be undertaken.

The energy requirements of the system can become excessively large when compared to local energy requirements, as such it may be the case that additional electricity infrastructure should be installed. The effects of these power lines should be reduced as it may affect the operation of the system and the nearby SKA structures. The energy requirements, keeping in mind the current energy capabilities of the local provider (Eskom) should be considered and an approach which utilizes and installs PV systems to reduce the load on the local power systems should be considered.

The physical components used in the array and data centre should all comply with local RoHS standards [6], this includes the use of lead free solder and all waste materials should be properly disposed of through the correct channels.

The introduction of large (non-ionising) radiation into the atmosphere should be clearly defined as this amount of power can be harmful to living organisms if exposed.

B FUTURE RECOMMENDATIONS

There are a number of characteristics of this system which fall short of a sufficient design. The first of these is the simplifying assumptions that are used in order to estimate the ability of the system. The losses throughout the system are likely to be larger than those stated in this report.

Due to the fact that the system is likely to be installed near to the SKA installation, this will prove to be difficult to implement without affecting their systems, however, the benefits of linking up with the SKA (to acquire land and spectrum rights) far out weight the difficulties.

The system has a small duty cycle, this implies that the instantaneous power required by each antenna will become large, this increases the cost of the system as each antenna is required to be built to a much larger specification than its average power consumption implies. This higher power requirement will consequently increase the costs of the transmitter. The pulse width is relatively small, which results in a range resolution of 1.5 km which appears to be relatively large. This implies that the system will fall short when multiple objects are in its view as it will not be able to distinguish between the two.

The maximum steering ability of the system is set to 30° which is a relatively low value when compared similar systems which often can steer up to 60° without grating lobes being present [7]. This low steering ability limits the capability of the system to detect space debris. The larger the angle of steering the higher percentage of total objects that the system is able to detect.

The downside of having a data centre on-site is that the majority of the data produced by the system is unlikely to be available to the public as the cost of transmission of this data can become highly costly. It may be feasible for systems to be designed such that physical shipping of data sets to be possible.

The current design does not go into much detail on the process of construction of such a design, as such some of these costs are estimated and may be different to an actual implementation. A further investigation into the physical construction and implementation in the real world should be carried out in order to gain a better estimate on the costing and feasibility of the system.

The implementation of the amplitude tapering may become complex as it requires a large amount of control out of the transmit amplifiers, they should be capable of dynamically varying their output powers while keeping harmonic distortion low while operating efficiently.

C BACKGROUND TO SPACE DEBRIS

This space debris was not thought to be an issue to the world at large as the belief was that space is immense and so there were no issues with using it as a dumping ground. It was not until the realisation by Kessler that the world began to worry [8]. This theory predicted that as the number of man made satellites (and other objects) in Earth's orbit increased, so did the probability of collisions between them. When orbiting debris collide, the two objects can fragment (due to the excessive relative speeds with which the two objects travel at) and cause multiple cascading collisions. This means that the debris orbiting the Earth would increase and result in greater difficulty for active space craft to undertake their missions. Protecting active missions from this space debris is highly difficult as it is challenging to predict the density of objects in the specific orbit that the missions' device should be in.

Guidelines were developed by NASA in the late 70's, however, this simply slowed the rate of introduction of debris, this did nothing to reduce the currently orbiting debris [9]. Recently, the United Nations General Assembly managed to get agreement between a number of countries to reduce the introduction of this debris [10].

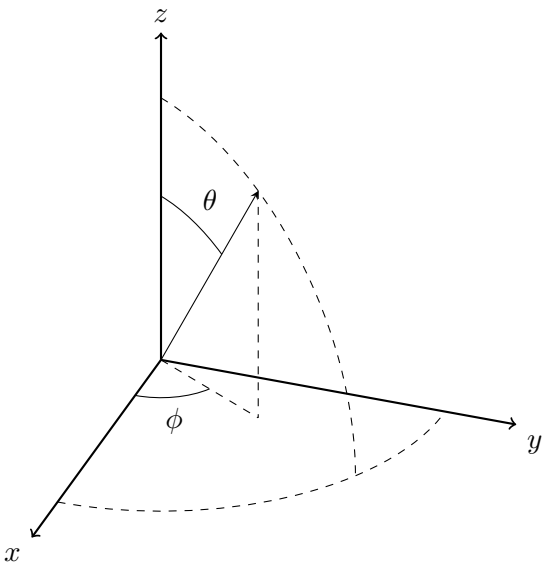

Figure A1: Coordinate System

There have been a number of methods created to deal with this issue. The first is to protect the current missions from this debris, in this case, make use of a Whipple shield, this is simply an outer coating of space craft that is able to protect the craft against high velocity impacts of objects in outer space [11]. This shield is built to protect the space craft from impacts from micrometeoroids in space. This method falls short when the debris becomes large enough to penetrate the craft (and the Whipple shield), resulting in the destruction/damage of the craft.

A recent system is capable of removing debris from the Earth's orbit, however, this is still in its early stages and has yet to prove highly effective [12].

D COORDINATE SYSTEM

The coordinate system used throughout this design report the coordinate system used is illustrated in Fig. A1, this is the spherical coordinate system.

E SPACE DEBRIS PARAMETERS

As discussed in section 1., space debris in Earth's orbit has been increasing for many decades, this is mainly due to space missions with poor regulations on the material that is allowed to stay in Earth's orbit. The majority of space debris is currently made up of man made air craft components, this includes objects such as: functioning space craft, non-functional spacecraft, rocket bodies, exhaust products, objects created through deployment operations, and products of deteriorated space craft [13]. Consequently, a large amount of this debris is made up of metallic materials as these materials make up the majority of the space crafts' components. It has, in the past [14], been difficult and costly to retrieve the components which were used to get the space craft into orbit, this is a major contributor to the material. This debris can occupy a number of regions within the Earth's orbits and this changes its characteristics.

The current scope of the project is that it should be capable of tracking space debris that is within the Low Earth Orbit (LEO). This orbit is defined to be approximately 160 km to 2000 km altitude above the Earth's mean sea level.

The second definition of these orbits is based on orbital mechanics, this states that if an object is within an orbit, then it will have a corresponding velocity. This is illustrated by equation 13.

$$V_{Object} = \sqrt{\frac{GM_{Earth}}{r_{Earth} + r_{Altitude}}} \tag{13}$$

Where:

- V_{Object} is the radial velocity of the object
- G is the gravitational constant ($6.67408 \cdot 10^{-11}\ m^3 kg^{-1} s^{-2}$)
- M_{earth} is the mass of the Earth ($5972 \cdot 10^{24}\ kg$)
- r_{Earth} is the mean radius of the Earth
- $r_{Altitude}$ is the altitude of the object above the mean radius of the Earth

This allows for the simple calculation of the minimum and maximum orbital speeds expected from the objects which correspond to the maximum altitude and minimum altitude respectively. These are illustrated in table 6. The velocity in the table is stated as a tangential velocity as it is assumed that the radial velocity of the object is zero. If an object has a radial velocity component, then this implies that it is changing orbits (an object in a specified orbit will have zero radial velocity) and this is either taking place due to a force acting on the object (man made) or it is experiencing a force due to the Earth's atmosphere. The vectors which explain this movement of an object is illustrated in Fig. A2.

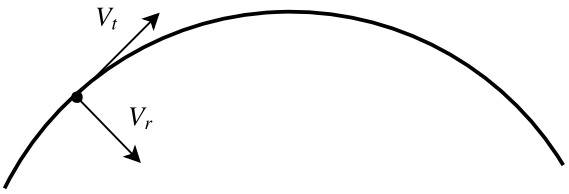

Figure A2: Object Velocity Vectors

The objects orbiting within these ranges have corresponding periods (amount of time it takes for an object to orbit around the Earth once), this means that an object in the lower orbit has a higher period than that of the higher orbits. The periods for the two limits of the LEO objects are listed in table 6.

Based on a number of physical limitations, the system implemented is only capable of detecting the space debris once it appears within the field of view (FOV). The FOV is discussed in section 7.1. Fig. A3 illustrates the system and its relation to the Earth.

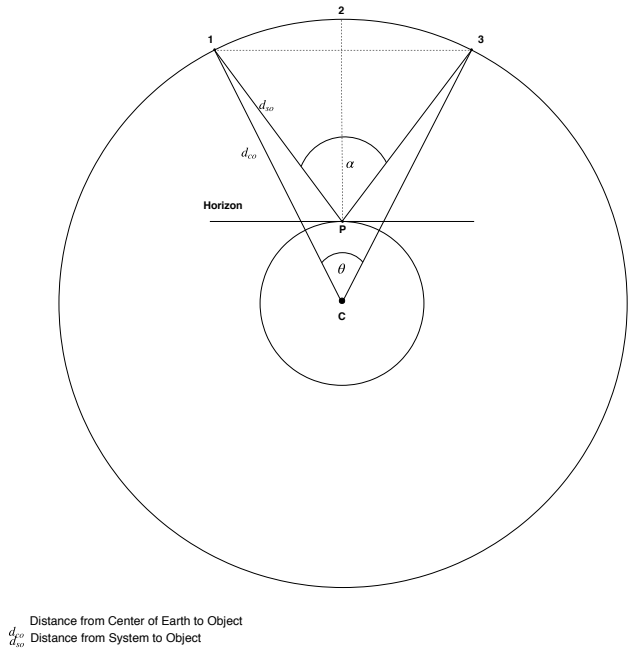

Figure A3: Observable Characteristics

The inner circle represents the Earth's surface and point P represents the position of the system on the Earth's surface. The outer circle represents the path of an object orbiting the Earth.

The lengths in this image are not to scale, however, this is used for illustrative purposes.

It is highly important to determine the amount of time it takes from when the object first enters and then exits the systems FOV. In this case it is assumed that the object travels directly over the boresight of the system and so it takes take the maximum amount of time to travel over the field of view. In most cases, the objects do not travel directly over the FOV, and will therefore be within the FOV for a reduced amount of time. This has a number of consequences for the capability of the system to detect objects, most importantly, the number of pulses that the system can use on an object as it moves over the viewing area.

This illustrates the system in order to create a few starting assumptions/criteria for the system. As can be seen in this image, the angle that is measured can be taken from two different reference points: the centre of the Earth and the point P. Based on this, it can be seen that the angles that these two points create are different. This implies that if one were to calculate the maximum distance that an object can be detected (assuming a maximum FOV angle from point P), one cannot make use of the angle α and the distances of this arc as it would not represent the actual distances of the objects because the circle that the object orbits around is different to the circle that is assumed the system makes use of. Numbers 1 and 3 represent the points at which the object enters and leaves the FOV, and point 2 represents the position of the systems zenith (boresight).

The calculations in this section make use of an average mean Earth radius, this implies that the observer is positioned at approximately sea level, this is unlikely to be the case for the placement of the system, however, the maximum altitude of feasible locations within South Africa are unlikely to exceed $\sim 1500\ m$, this change in distance will provide a negligible difference to the calculated values and final design of the system.

Based on the movement of objects in differing orbits, it can be seen that objects in higher orbits move slower than those in lower orbits. The objects move with a specific velocity, as illustrated in table 6, this is measured in linear velocity, however, it is also important to represent the motion of

these objects with the use of their angular velocity, the angular velocity is simply found with the use of equation 14.

$$\omega = \frac{v}{r} \tag{14}$$

Where:

- ω represents the angular velocity of the object (Radians per second)
- v represents the linear velocity of the object
- r represents the distance from the observer to the object

Once this has been estimated, it is important to evaluate the angle travelled by the object as seen from the observation point (α_p). This is measured over a period of time (ΔT) and the angular velocity calculated above (ω_P) is used, this is found in equation 15

$$\omega_P = \frac{\theta_P}{\Delta T} \tag{15}$$

Where:

- ω_P is the same as before
- θ_P represents the angle of the object seen from the observation point
- ΔT represents the amount of time that it takes the object to traverse the angle

This now allows for the calculation of the linear velocity of the object as seen from the observation point (it is the same if the centre of the Earth is used as the reference point). This velocity is calculated with the use of equation 16.

$$v = \omega_P h \tag{16}$$

Where:

- v is the linear velocity of the object (m/s)
- ω_P represents the apparent angular velocity of the satellite (Radians)
- h represents the altitude of the object

The use of the two equations above require the values for the amount of time that it takes for an object to enter the FOV of the system and exit it again. This is found with the use of equation 17 [15].

$$t_t = \frac{r^{\frac{3}{2}}}{\sqrt{GM}}(\pi - 2E - 2asin(\frac{R}{r}cos(E))) \tag{17}$$

Where:

- t_t is the amount of time that an object is in the FOV of the system
- r is the geocentric distance of the object (distance of the object above mean sea level)
- G is the gravitational constant
- M is the mass of the earth
- E represents the elevation of the object above the horizon of the system

The elevation of the system is important as it relates to the FOV of the system. The two are interrelated by the fact that the elevation angle is the complementary angle of the maximum FOV of the system. This implies that if the elevation of the system is known, then the FOV of the system can be calculated.

Table 6: Object Parameters

Parameter	Value
Minimum Object Altitude	160 km
Maximum Object Altitude	2000 km
Minimum Object Slant Distance	184 km
Maximum Object Slant Distance	2223.8 km
Minimum Object Tangential Velocity	6897.4 m/s
Maximum Object Tangential Velocity	7807.9 m/s
Minimum Angular Velocity	0.0034 rad/sec
Maximum Angular Velocity	0.0488 rad/sec
Elevation Angle (assumed for illustration)	60°
Angle (Measured from Zenith)	30°
Maximum Observable Time	323.37 s
Apparent Angular Velocity	0.0032 rad/sec
Minimum Linear Velocity	518.14 m/s
Maximum Linear Velocity	6476.8 m/s

In table 6, the elevation angle is assumed to be approximately 60°, this is a first estimate of the FOV of the system, further analysis of the system FOV is discussed in 7.1. This elevation angle refers to the maximum amount of time that the object is visible. This implies that the object travels directly over the boresight of the system. In most circumstances, the objects will not travel directly over the boresight and will therefore be within the FOV for less time than stated in this table.

This creates the ability to calculate the observed velocity of the object as it passes over the FOV of the system, this is illustrated in Fig. 18.

$$v = \omega_P h \tag{18}$$

Where:

- v is the linear velocity of the object (m/s)
- ω_P represents the apparent angular velocity of the satellite $(Radians)$
- h represents the altitude of the object (m)

In addition to this, with an assumed elevation angle, the expected distances for the objects can be found, these are calculated making use of equation 19 [15].

$$\rho = R\left(\sqrt{\frac{r^2}{R^2} - (cos(E))^2} - sin(E)\right) \tag{19}$$

Where:

- ρ is the slant distance from the system to the object (m)

The other parameters are taken as used in equation 17. This equation is important as it provides another criteria for the system, that of the maximum range that is required to be detected by the system. These become important for the Radar Range Equations (RRE) in section 4.2.

E2 Space Debris Physical Characteristics

Now that a number of key characteristics of the movement of the objects have been calculated, it is important to detail the sizing and physical characteristics of the objects that are evaluated.

There are multiple ways in which to model the space debris that is being tracked. This includes parameters such as: electron density, ion composition, electron drift velocity, etc. This in depth analysis of the debris is out of the scope of the project and a few simplifying assumptions are chosen for this section of the report. The first of these is to assume that the system is only required to detect *hard* targets, this refers to the fact that the object is a solid and has a predictable characteristic when reflecting the EM waves incident on it. The *soft* targets include ionospheric plasma present in the atmosphere, these targets are not important to this report [16].

Based on current implementations of space debris trackers, an assumption is created here that the minimum RCS of an object is assumed to be that of 10 cm in diameter. As discussed in the above section, the objects in question are assumed to lie within the LEO; objects that are below this range experience force due to the atmosphere and therefore will slowly lose orbital velocity and will eventually fall into the Earth's atmosphere and (commonly) burn up in the process. The majority of the objects lie within the 500 km to 1000 km altitude band, after this point, the density of objects decreases [17].

The information provided in the sections above create a baseline with which to design the system.

F CURRENT IMPLEMENTATIONS

The first of these is the Advanced Modular Incoherent Scatter Radar (AMISR), this is located in Resolute Bay, Canada, it makes use of an array of crossed-dipole antennas that are electrically phased, the system is electronically steerable. It operates in the frequency range of 430 MHz to 450 MHz and has a pulse width of approximately 2 μs [2]. A number of important parameters can be found in [2], this is a system which closely resembles the major requirements for this system. The second system in use by Leo Labs is the Midland Space Radar (MSR), this system is located in Texas and is commissioned by Leo Labs, this system is capable of detecting objects as small as 10 cm in diameter. It is not specified whether this value is a Radar Cross Section (RCS) or the physical size of the object. A number of other implementations have been used (not through Leo Labs) which make use of other technologies and are capable of detecting smaller objects [3, 18–22]. A number of these papers are made use of to design the system in this report.

G RADAR THEORY OF OPERATION

This section details the different implementations of radars that are capable of detecting objects and the characteristics of those objects when detected (speed, direction, distance, etc.).

Sections G1, G2, G3 discuss the theory of operation of the system.

G1 Monostatic versus Bistatic

There are two major radar configurations that are currently used, these two are discussed below and then compared.

G1.1 Bistatic The bistatic configuration makes use of a separate transmitter and receiver in order to implement the system. The two components are placed at differing locations and the separation between the components is required to be sufficiently large in terms of the angles or ranges that they present [21], [23, p. 5], [24, p. 3]. The separation between the transmit and receive systems allows for minimal interference between the two, while allowing for the use of more than one receiver.

This implies that the two systems, in the case of Earth-to-Space transmission, are required to be geographically (in the order of kilometres) far apart [25]. The transmitters in these systems generally transmit power in the range of kilowatts to megawatts, this is in order to increase the SNR of the system as there is a significant amount of energy lost in the energy transfer process. The receiver on the other hand, works with milliwatts to nano Watts as it receives this greatly reduced power that is reflected from the objects in question. The bistatic system provides a convenient method of separating out the two systems such that it becomes increasingly difficult to damage the receivers' equipment from the high power generated by the transmitter. This mode of operation allows for the calculation of the distance of the target to the receiving antenna, however, the calculations involved for this are more complex than for the monostatic case, the same applies to the doppler shift measurable by the system.

G1.2 Monostatic The other, more commonly used system, is the monostatic configuration. This bundles the transmitter and receiver together on the same antenna/antenna array. The nature of this system is such that the transmitter and receiver are required to be isolated while the two transmitting and receiving actions are taking place. The isolation can be carried out in different ways, a circulator or a switch commonly achieves this. In many designs, there are multiple levels of protection for the receiver, as this component is commonly expensive and highly sensitive. These components are discussed in section 7.6. In the monostatic configuration, the transmitter and receiver do not operate at the same time which greatly simplifies the switching apparatus. This mode of operation allows for direct measurement of distance of targets as well as the ability to measure the targets radial velocity (with respect to the observation point).

G1.3 Comparison The configuration designed for this system is the monostatic as it provides a lower cost alternative to the bistatic configuration. It has the added benefit of only requiring one piece of land for the systems implementation. The system cost is lower than the bistatic case based on the fact that only one set of antennas are required. There are cases where the monostatic system can be set up with two sets of antennas (for transmitting and receiving), where the separation of the two installations creates a small angle. The bistatic configuration is easier to implement with regards to the protection systems for the receiver, however, this benefit does not out weigh the monostatic systems advantages. The bistatic systems also require a complex communication ability between the two locations which increases the cost of implementation, most notably when the distance between the two systems is large and communication mediums can become prohibitively expensive.

G2 Continuous Wave and Pulsed Wave

The two commonly used transmission methods are the continuous wave and the pulsed wave, these two systems are also linked to the choice on the system configuration. This implies that if the monostatic configuration is used, then the continuous wave transmission system is not available.

G2.1 Continuous Wave Transmission The continuous wave transmission system, as the name indicates, has the transmitter functioning 100 % of the time, which implies that the receiver also functions 100 % of the time. The continuous wave transmission system, as indicated above can only be used by the bistatic configuration as the receiver cannot be activated while the transmitter is active. A unique characteristic of the continuous wave system is that it is unable to determine the electromagnetic (EM) waves' round-trip time as there is no set begin and end time of transmission. This can be solved with the use of modulation on the wave, which requires the receiver to know all of the characteristics of the transmitters' waveforms ahead of time if it is to determine round trip times [26, p. 20].

G2.2 Pulsed Waveform Transmission The second method of EM wave transmission makes use of pulses, these occur periodically and their duration is commonly over a short period of time. This system is commonly used in tandem with a monostatic configuration and this provides the ability for components to afford isolation between the transmitter and receiver circuitry. Following the EM wave pulse, the receiver is set to record the resulting EM waves that are returned in the form of echoes after it has reflected from the objects in question. The determination of the pulse length and the period between pulses (the inter-pulse period (IPP)) is discussed in section 4.2 as this value is dependent on a number of other characteristics of the system. The pulse repetition is also linked to the observable time window of debris, discussed in section E1.

G3 Threshold Detection

Once the system has transmitted an EM wave and the echo has been received, this energy received is analysed to determine if an object was detected, and what its characteristics are. In order to detect a signal, the received signals' power is required to be above a specific threshold. This threshold is defined as the level at which all sources of noise are incorporated and accounted for. When an object is detected, the signal level is required to rise above this threshold and this is then considered a successful detection.

There are cases, based on the fact that noise is inherently a random variable, that the noise level can exceed the threshold set by the system. This is observed as a false alarm [26, Ch .3]. This implies that there are cases where the targets echo in addition to the noise are capable of being below the threshold, this is when the noise in the system is low, so the addition of the echo is not large enough for the system to detect the object. These two cases are highly unlikely, however, cannot be ignored as they are based on the probabilities of the entire system.

These probabilities are given as two variables: the probability of detection (P_D), and the probability of false alarm (P_{FA}). The probability of detection is the probability that an object-plus-noise exceeds the threshold applied to the system. The probability of false alarm is the probability that the noise (from all components of the system) will exceed the threshold. The best case scenario for these two variables are:

$$P_D = 1 \tag{20}$$

and

$$P_{FA} = 0 \tag{21}$$

These values are idealistic and so the correct threshold value is required to be set such that the system can operate as close to these values as possible. When the threshold is increased, the probability of false alarm will decrease - however, so will the probability of detection. When the threshold is decreased, the probabilities of both variables increase. A trade-off is required here to determine the optimum threshold level.

There is one way in which to increase the probability of detection while lowering the probability of false alarm, this is achieved by increasing the targets signal power (it should be noted that the signal power should be increased relative to the noise power). The method in which this can be accomplished is to increase the overall Signal-to-Noise-Ratio (SNR) of the system, if the overall SNR is increased above a specified level, then the probabilities discussed above, reach levels that adequately satisfy the criteria of the system. The SNR and how it is attained is discussed in section 5.

H FREQUENCY ALLOCATION

The following sections detail a number of considerations while selecting a frequency, and how this process will be carried out.

H1 Political and Economical Limitations

In addition to the reasons discussed in section 3., a further factor that affects the frequency band choice are those frequencies available by the systems regulator. The current communications authority of South Africa is run by ICASA [27], who keep an updated list of the currently used frequency bands and the regulations that the operators should adhere to [28], this document is used in order to determine the optimal frequency band. The frequency allocation within a country is highly regulated, and as such it becomes costly to demarcate specified frequency bands for specific uses. The first criteria for the choice of a frequency band is the current usage of the frequency band, the request for in-use bands can expand the budget of the system greatly.

The method used to determine the optimal frequency band is to first define the search range (200 MHz to 1 GHz, from above), from this point, the frequency bands that are commonly allocated to astronomy research are narrowed down. The frequencies which lie within this area of interest are: $406.1 - 410\ MHz$ and $606 - 614\ MHz$. The first band has a bandwidth of 4 MHz, whereas the second has an 8 MHz bandwidth. The larger bandwidth is highly beneficial for the system as there are lower chances of bandwidth bleed-over from other systems, the ability to make use of a larger bandwidth (if required) and, in addition to these two facts, this frequency band is used as a primary basis for radio astronomy. This gives a higher likelihood that the systems regulator will grant the frequency band for this usage, as it falls within its intended usage. The bandwidth that this allocation allows is unlikely to be completely used by the system designed, this is due to a number of constraints, namely, the Doppler effects, and the pulse width that the system will make use of.

In the case that an entity wishes to make use of a frequency band within South Africa, a number of rules are applied to the entity as well as a number of costs for the use of the frequency band (depending on the selected one), these costs can become highly prohibitive as well as being highly difficult to find a band where there is little to no interference. As discussed in the previous section, interference is a massive concern for the choice of frequency, this is why the frequency choice, as well as the location of the system are inherently linked.

The choice of location of the system is highly relevant as the interference from external sources can severely affect the ability of the system to function. The first major way in which to avoid these possible interferences is to locate the system in a low population density area. An area with a low population density implies that there will be a lower saturation/use of power over the frequencies of interest.

The first part is to determine the area of South Africa with the largest area and the lowest population density. The province which satisfies this criteria is the Northern Cape [29, p. 18], as it has the lowest population of any province, it also has the largest land area [30, p. 9,15]. This allows for an efficient placement of the system with regard to the frequency of interest.

In addition to the fact that placement in the Northern Cape is beneficial, the Square Kilometre Array (SKA) is also currently located in this province. The development of the SKA has required the implementation of a set of special by-laws which apply to the areas within the province. These by-laws are discussed in the following sections.

Due to the fact that the SKA requires an extremely low noise environment in order to undertake its scientific research, it has permission to demarcate specified areas of land for scientific research [4]. The minister has the ability to declare any area or part of an area in the Province of the Northern Cape as an astronomy advantage area. This implies that an area, which is technically advantageous to the functioning of the system can be demarcated by this act. This implies that, within demarcated areas, the SKA is able to allocate specific frequency bands to particular projects/entities. The act enables the purchasing process of land to be facilitated by the National Research Foundation (NRF) which can greatly simplify the process of determining a location for the system. The act prohibits the use of specific frequencies within these areas, this is highly beneficial for the system as it reduces the noise introduced from external factors.

Collaboration between the SKA and this system can be highly beneficial, the scientific research community will be given access to the system on a periodic basis. In order for the SKA to allow this system to be used within the Northern Cape, it should be created such that it does not interfere with their systems and still be of benefit to them. In addition to the requirements of the SKA, a number of other considerations are required to take place: local affected businesses, affected agricultural tenants/owners, environmental impacts, nearby electrical and radio interference. A number of these concerns are discussed in section A3. The act allows for the allocation of required frequencies (regardless of the frequency allocation of ICASA) [31]. The permits provided by the act create exemptions for the frequency spectrum that is permitted.

The location of the system is discussed further in section P where a number of environmental factors are discussed.

I POWER DENSITY DERIVATIONS

The first equation which defines the power incident on a target, is given by equation 22. This power is generated with the use of the antenna array, the details of this array are discussed in section 7.

$$P_{inc} = P_t \cdot \frac{G_t}{4 \cdot \pi \cdot R^2} [W/m^2] \tag{22}$$

Where:

- P_{inc} is the power incident on the target (W)
- P_t is the power transmitted from the system (W)
- G_t is the gain of the system (dB)
- R is the distance from the system to the target (m)

This equation assumes the use of a directional antenna (not isotropic) which has a corresponding gain which allows for the concentration of the beam in a specific direction.

The next stage is to determine the magnitude of energy that is reflected by the target, as assumed in section E2, the radar cross section of the target is defined and known.

Equation 23 indicates the magnitude of power reflected by this object.

$$P_{refl} = \frac{P_t G_t \sigma}{(4\pi) R^2} \tag{23}$$

Where:

- P_{refl} is the reflected power from the target
- σ is the radar cross section (RCS) of the target measured in square meters (m^2)

This reflected power from the target is then received by the system and this is defined by equation 24.

$$P_r = \frac{P_t G_t G_r \lambda^2 \sigma}{(4\pi)^3 R^4} \tag{24}$$

Where:

- P_r is the received power at the system (W)
- A_e is the effective aperture of the system (m^2)
- λ is the wavelength of the system (m)
- G_r is the gain of the receive antenna (dB)

It is assumed that the gain is determined with equation 25.

$$G = \frac{4\pi\eta_a A}{\lambda^2} = \frac{4\pi A_e}{\lambda^2} \tag{25}$$

Where η_a is the efficiency of the antenna created which is commonly between 0.5 and 0.8 [26, p. 64].

In the case of the monostatic antenna array, the transmitting and receiving gain are the same as it is the same array. This implies that for bistatic systems, it is possible to have two different ranges for receiving and transmitting [26, p. 64].

J PROBABILITY OF DETECTION

As discussed in section G3, the act of detecting an object is probabilistic which means that the system should be designed in such a way as to increase the probabilities of detection. The first part of this is to make use of equation 26 in order to map a selected set of probabilities to a required SNR value [26, p. 107].

$$SNR(dB) = -5log_{10}N + \left(6.2 + \frac{4.54}{\sqrt{N + 0.44}}\right) log_{10}(A + 0.12AB + 1.7B) \tag{26}$$

Where

$$A = ln\left(\frac{0.62}{P_{FA}}\right) \tag{27}$$

and

$$B = ln\left(\frac{P_D}{1 - P_D}\right) \tag{28}$$

This set of equations is used to generate Fig. A4 (in this case N is the number of pulses, which is assumed to be 1).

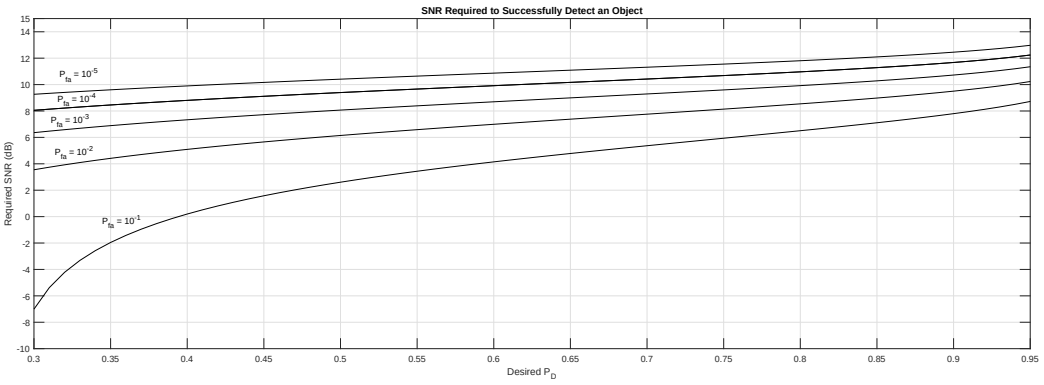

Figure A4: SNR Required for Detection

This implies that in the case that for realistic values for the two probabilities, the SNR required reaches a value of approximately 10 dB. This is therefore defined as the minimum SNR (SNR_{min}) required for the system to function. Based on this equation, it can be seen that if the number of pulses is increased, then the SNR required will become lower. This current approximation makes use of a single pulse on a target. The affects of increasing the number of pulses here is not included within the calculations in order to simplify part of the design process. However, the effects of increasing the number of pulses should be included in in-depth calculations as it can affect a number of design decisions. Selecting the number of pulses has been undertaken in a simplified manner in section 5.1 in order to attain a simplified analysis, however, this value is highly variable and is affected by a number of circumstances and conditions and also how the system is operated in reality.

This first estimate for the minimum SNR required is linked to the noise present in the system, the noise of the system is evaluated in sections 5.2 and 5.3.

K VSWR AND RETURN LOSS DERIVATIONS

The Voltage Standing Wave Ratio (VSWR) is an important parameter for any antenna, this is the characteristic which determines the ratio of the input signal which is reflected to what is transmitted. This value should be as low as possible, it ranges from 1 (complete signal transmission) to infinite (complete signal reflection). These correspond to a perfect match and a perfect mismatch respectively. A VSWR value of lower than $1.3:1$ is sufficient for this application as this represents a return loss of $-17.7\ dB$ [32–35]. This value is a compromise between cost and antenna performance. Lower VSWR values become difficult to achieve as the price becomes prohibitive. This value is attained based on current implementations of these types of antennas and their specifications. This VSWR results in a low reflection back into the amplifier (and consequently reflection that doesn't enter the antenna when in receiving mode).

The parameters illustrated above are calculated with the use of equations 29, and 30.

$$VSWR = \frac{1 - |\Gamma|}{1 + |\Gamma|} \tag{29}$$

$$ReturnLoss(dB) = -10log_{10}\left[\left(\frac{VSWR - 1}{VSWR + 1}\right)^2\right] \tag{30}$$

Where the reflection coefficient, $\Gamma = \frac{Z_L - Z_0}{Z_L + Z_0}$ and Z_L is the load impedance and Z_0 is the characteristic impedance.

This VSWR value defined here is linked to the bandwidth of the antenna, as this VSWR will not be maintained over a large frequency range. In this case it is useful to define a maximum VSWR over the frequency range of the antenna. The design for this is such that the VSWR is less than $2:1$ for the bandwidth of the antenna (and the system as a whole).

L CROSSED DIPOLE

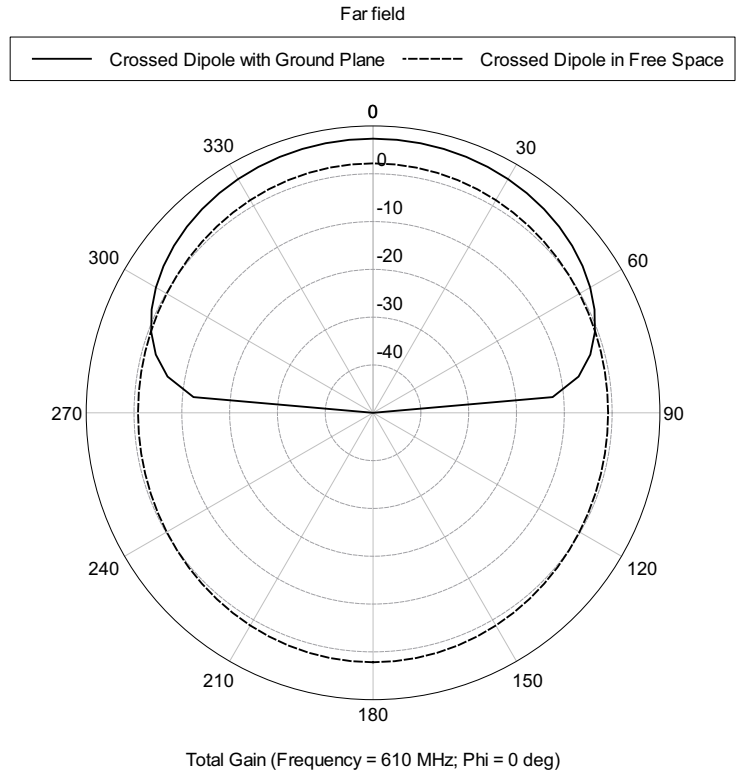

Figure A5: Crossed Dipole Polar Plot

Table 7: Crossed Dipole Comparison

Parameter	Crossed Dipole (free space)	Crossed Dipole (ground plane)
Maximum Gain (dBi)	2.175	7.340
Maximum Gain Direction (degrees)	0	0
Minimum Gain (dBi)	-0.835	$null$
Minimum Gain Direction (degrees)	± 90	± 90
Half Power Beam Width ($-3\ dB$)	N/A	100.401

M ELEMENT SPACING DERIVATION

In order to avoid the grating lobes, the separation between each consecutive element in the array should not be multiples of the wavelength of the antenna [36, p. 297]. In order to eliminate this probability, the spacing between elements should be less than one wavelength.

In order to achieve this spacing, the antennas are rotated by $45°$, this allows for tighter packing of the antennas. This configuration is illustrated in Fig. 3b, this is for a 2×2 array, the illustration is from above the array (birds eye view).

This creates a manageable spacing between the elements such that they can be easily installed and will

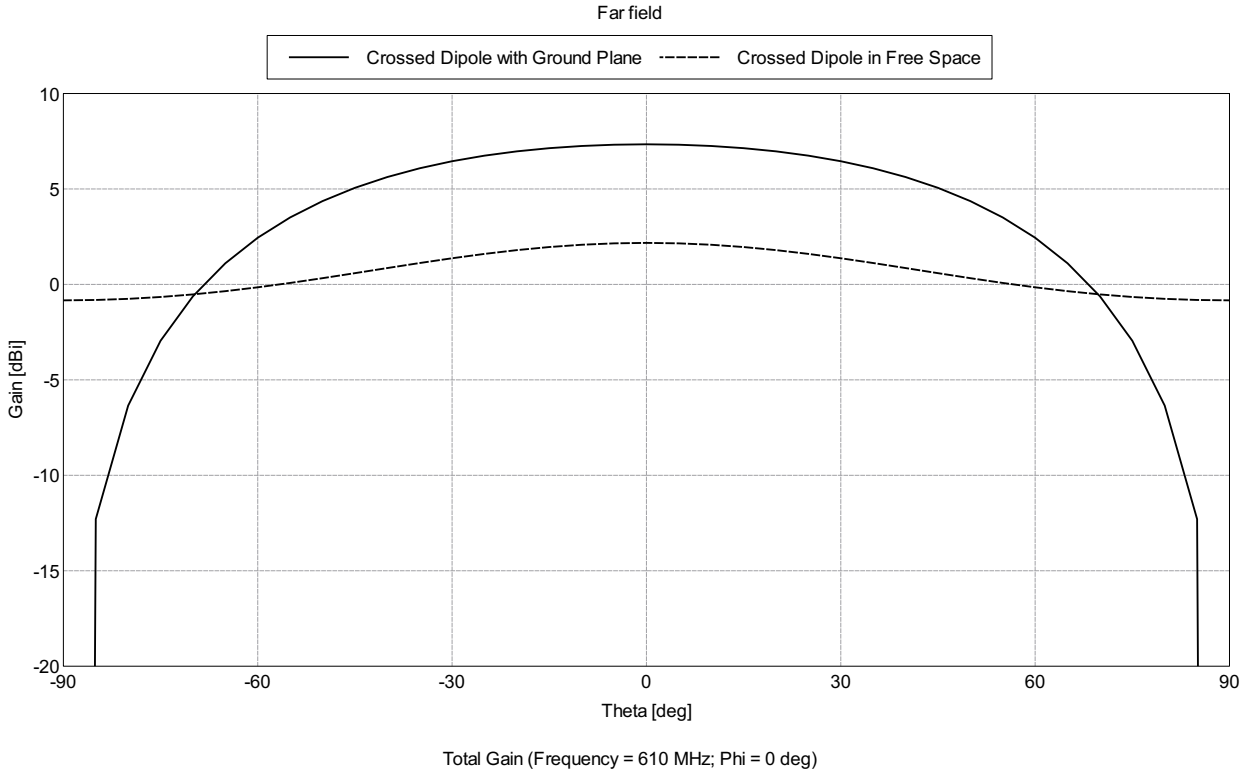

Figure A6: Crossed Dipole Cartesian Plot

not interfere with adjacent antennas (mechanically). This is also important for cases where antennas need replacing, this makes this process easier.

The elements are spaced the same distance above the ground plane as for the single antenna. The ground plane is created with a conducting mesh. The mesh is created such that the spacing between each consecutive line is less than $\lambda/10$ apart. This spacing reduces the cost of the ground mesh as this ground mesh acts as a solid surface in reference to the frequency that is incident upon it.

A secondary method to prevent grating lobes is by specifying the element spacing (not implemented in this solution) where equation 31 provides the spacing [26, p. 331]. In this case, the maximum steering angle required is the parameter, θ, this results in a spacing that can be approximated by 0.75λ. This method of spacing the elements can reduce the cost of the overall array as it can result in the reduction of required antenna elements [26, p. 331]. The reason this was not used is based on the fact that a large amount of power is input to the system so increasing the number of elements increases the power experienced by each antenna which introduces more complexity to the design of the antenna as it then has to dissipate larger amounts of heat.

$$d \leq \frac{\lambda}{(1 + |sin\theta|)} \tag{31}$$

N GROUND PLANE CHARACTERISTICS

In this section, it is pertinent to note the difference between the use of a ground plane and the absence of a ground plane, Fig. A7 and A8 illustrates this difference in the case of a 32×32 antenna array.

Fig. 4, A8, A7 illustrate the different gains acquirable based on the sizing of the array and how the ground plane affects the system.

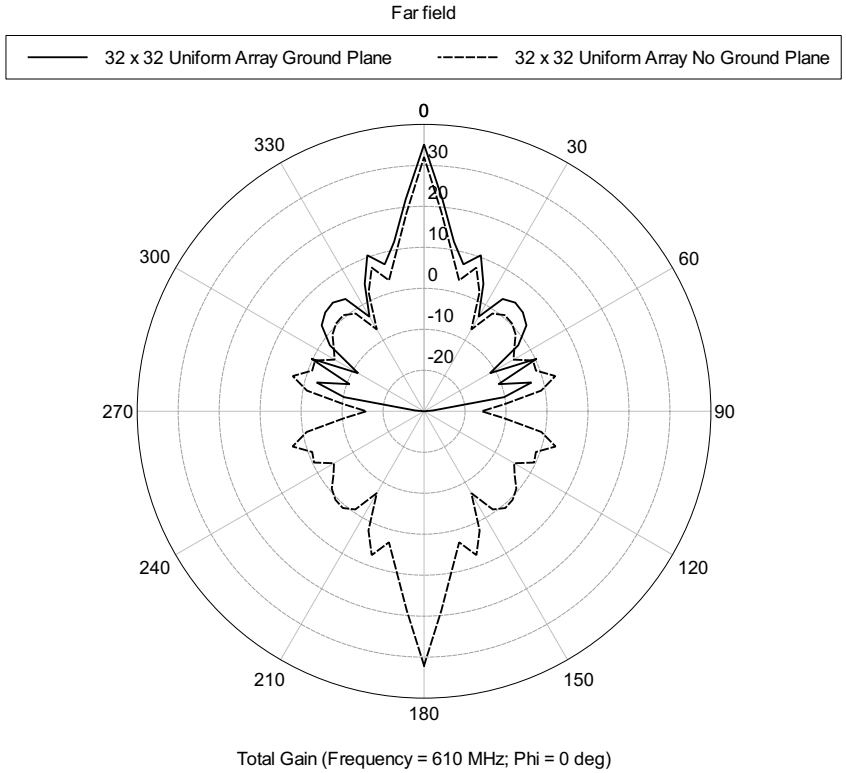

Figure A7: Ground Plane vs No Ground Plane - Polar Plot

O STEERING ABILITY OF 32×32 ARRAY

Fig. A9 and A10 illustrate the steering capabilities of the system for a 32×32 sized antenna array.

P ENVIRONMENTAL CONSIDERATIONS

The design of this system has considered the technical details of tracking space debris. In order to implement this in a real world situation the environmental factors are analysed in this section. Based on the choice of the frequency and how it is used, the location of the system is based in the Northern Cape where there is a low population density and a large area. This is highly important such that the system has as little radio interference as possible.

P1 Location

Subject to the choice of the frequency and how it it licensed, the array is situated within the Northern Cape (refer to section 3.). This is based on the fact that the SKA has the ability to provide a number of laws which allow for the selected frequency to be utilised within this province. The Northern Cape is a largely unpopulated area when compared to the rest of the country, implying that it has a low population density (as it has the largest area). This is convenient as it lowers the cost per area of land. Based on the spacing of the array, the size of land required should be at least 247 m^2 (based on the $\lambda/2$ spacing and the 64×64 array sizing), this is the minimum area required for the placement of the antennas. The system is equipped with a number of additional components which all take up space. This implies that the system is required to be housed with at least a 2000 m^2 plot of land, this implies that, based on the average cost of units of land of this size, the price will be approximately R 800 000 to R 1.2 million [37–39]. The price of the plot of land varies based on its location, previous owners, and proximity to towns. A pragmatic approach to estimating the cost of the required land is to take the maximum value stated here and add on an additional 20 %. The cost of the area of land is then approximated to R 1.44 million.

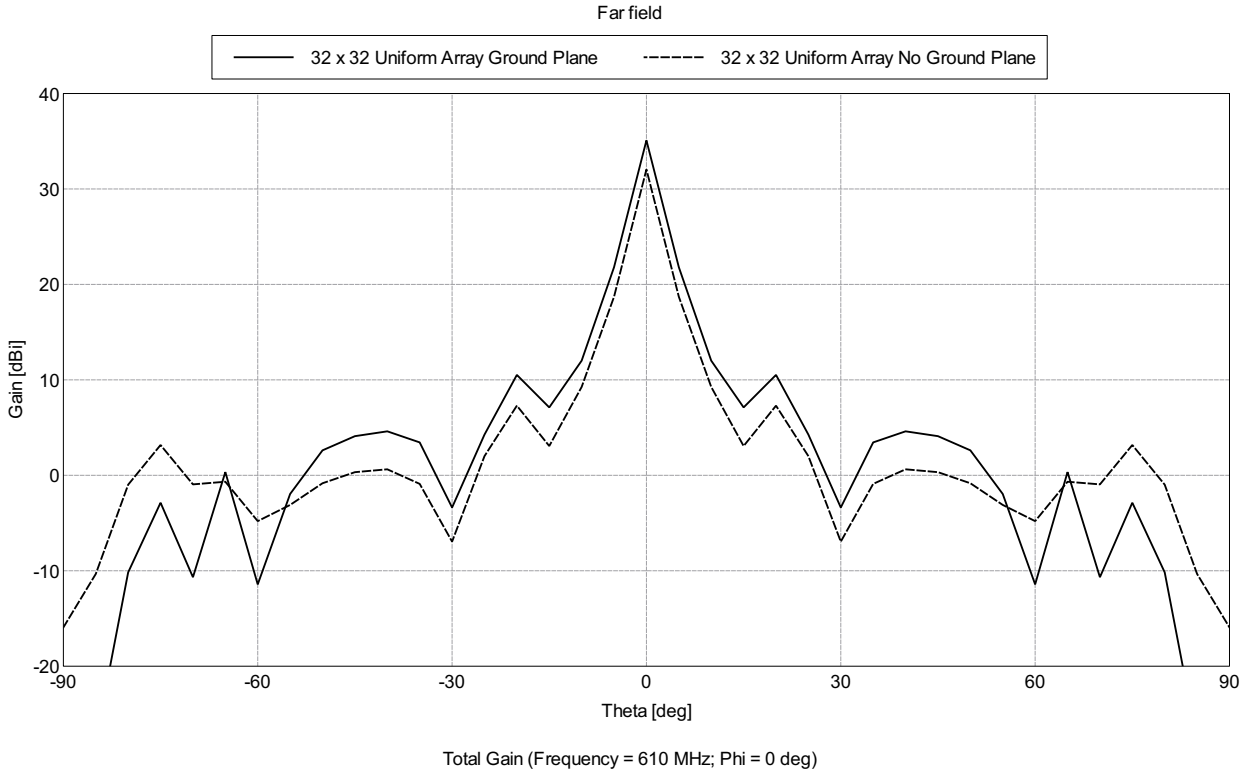

Figure A8: Ground Plane vs No Ground Plane - Cartesian Plot

The ideal location for the land would be within a short distance from the SKA operations, this results in the added benefit of the lowered radio interference from external sources while being able to cooperate with their operations. The SKA has currently build their own infrastructure for data management. Tying in with their system implies a lower cost for both parties as it can benefit both. The cost incurred for this communication platform can become expensive, an in-depth analysis should be undertaken as to how the data transmission mechanism should work. The first method is to make use of on-site servers which take all of the information directly from the array and apply analysis on this data, package the data, and send out the important characteristics that it has analysed. The second method is to automatically send out all of the data that is retrieved from the system, this data is then sent directly to an external server (a cloud provider such as Google, Amazon, etc.) and then the analysis is then carried out from this service. The cost of these two systems are required to be analysed as they both have benefits and drawbacks. The first method will require a large up front investment for the installation of the servers, then a recurring cost for the energy that is consumed for the analysis, this greatly reduces the costs of data transmission. The second method will have minimal up front costs, other than the recurring cost of the maintenance and rental of the data line, as well as the costs to analyse this data when it is stored on the cloud. The SKA ran a feasibility study to determine which of these methods is more cost efficient, their decision was to install an on-site data centre as the costs of installing a fibre line to transport the data far exceeded the installation costs of the data centre [40, p. 17-18]. This data centre will require the installation of an RFI shielded building such that the components inside do not interfere with the array [40, p. 18].

The power requirements for the installation of this system can become complex, in addition to this, the power transmission system should comply with the regulations of the SKA. The SKA undertook an investigation to the installation for power [40], this document highlights the requirements for the installation of power and how it is required to be routed so as to reduce interference with the measurement apparatus.

The plot of land is required to be relatively low gradient for the installation of the physical array as

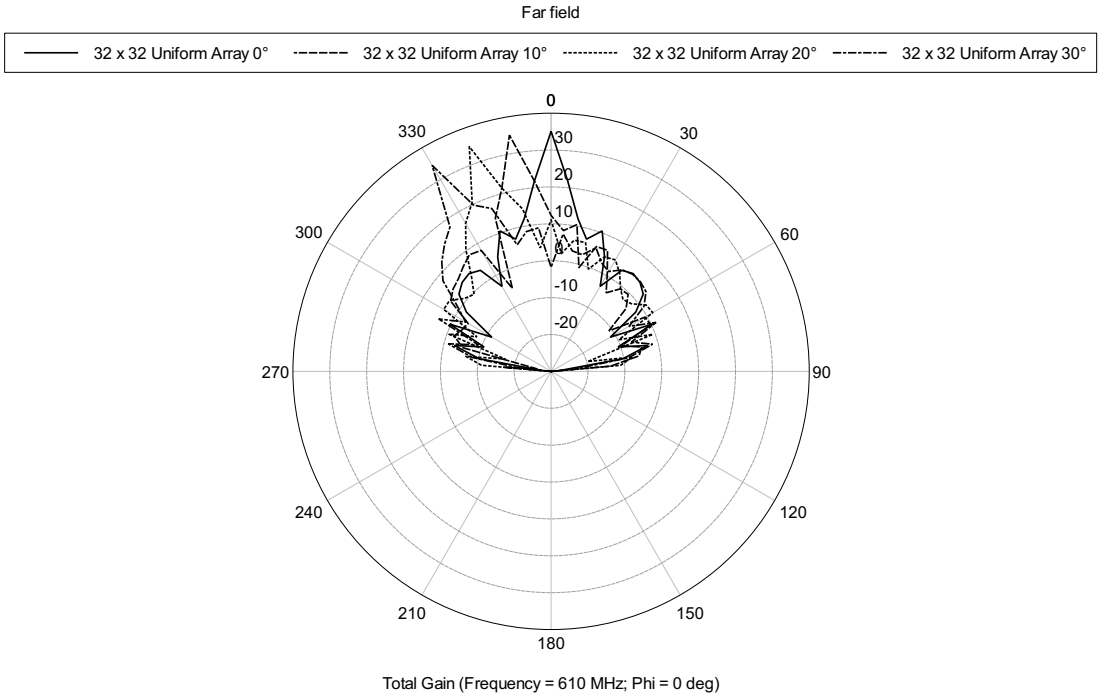

Figure A9: 32×32 Array Beam Steering Ability - Polar Plot

this is required to be mounted flush against the surface of the Earth and directed upwards. In order to install the system, an in depth analysis is required to be carried on the land, this analysis has been undertaken by the SKA in the local area (180 km radius)[40, p. 95,98], which concludes that the minimum depth at which the structure can be fixed is 3.5 m below the surface. The nature of the ground under the array can prove to be difficult to lay foundations for construction.

Due to the placement of the SKA, placing the system in close proximity implies that low flying aircraft are prohibited within the local airspace as this can affect the system. Local authorities should be notified of the implementation of this system such that regulations are put in place for flight paths that may be affected.

Depending on the site chosen, roads and standard infrastructure (water, electricity, etc.) may be required for the construction of the system, this increases the overall cost.

This system should be capable of functioning for a minimum of 40 years [41, p. 336], this is a standard requirement for large operations, as such it should be capable of withstanding the environment for this period of time. Section P2 analyses a number of concerns for the area of installation.

P2 Weather Dependence

The Northern Cape (specifically near Carvernon, where the SKA is situated) is at a relatively high altitude, it is also a semi-arid area with little rainfall throughout the year [42]. This is highly beneficial for the system as rainfall can severely affect the functioning of the system (due to the loss of EM wave energy by the water). The low humidity and rainfall is convenient for this system as this area is located above the rust belt (the border where corrosion from the sea air is reduced to negligible levels) of South Africa. This implies that the system will require little to no maintenance from corrosion over time.

The temperatures experienced during the Summer season in this area of the country often range between 34° C to 40° C. Frost and dew often occur during the winter months, this implies that the

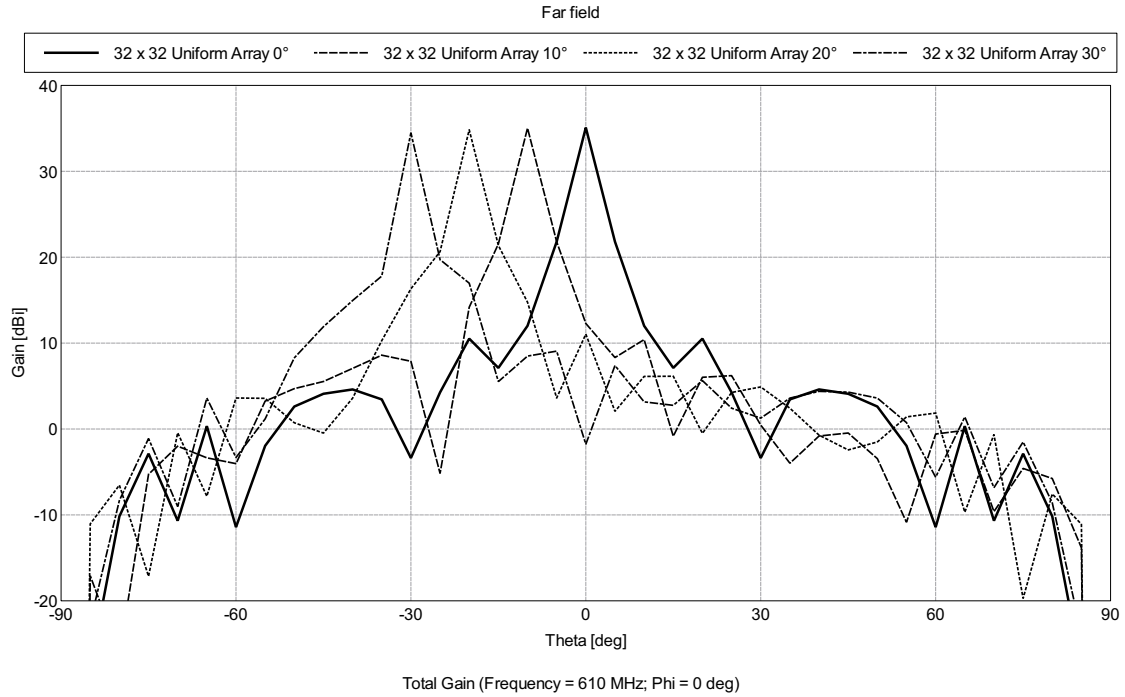

Figure A10: 32×32 Array Beam Steering Ability- Cartesian Plot

components should be designed such that they can handle extreme temperature swings.

Q TRANSCEIVER

The transceiver of the system is made up of the components of the transmitter and receiver, these two components are often separated in illustrations, and are discussed in the following two sections.

Q0.1 Transmitter The radar exciter is a simplistic system whereby a waveform is generated with the use of an oscillator, this signal is then amplified with the use of a high power RF amplifier. This is fed directly into the circulator.

Q0.2 Receiver The frequency utilised within this system is relatively large when considering the Analogue-to-Digital-Converters (ADC) currently available. The cost of ADC components which are capable of sampling this frequency are prohibitively expensive. This calls for the use of a frequency mixer (down-converter) such that the EM waves received by the amplifier are shifted down in frequency and are then sampled at that point. Once this sampling has taken place, processing of the data takes place to determine if detection has occurred. This implementation reduces the cost of each receiver system. The overall diagram of this is illustrated in Fig. A11. The transmitter part of the system is illustrated here as a block as it interacts with the system through the circulator. The local oscillators frequency is required to be relatively close to that of the system as the intermediate frequency (IF) output from the mixer [26, p. 397-398]. The implementation of a second mixing stage decreases the mixers intermodulation components which allows for easy filtering (removal) to get the final signal [26, p. 398]. The lower frequency signal created from this process is then easily sampled with a lower cost, high quality, ADC such that characterisation of the signals is possible. The detail of the mixing process is out of the scope of this design as the final IF frequency for sampling requires further calculation. The LNA is placed close to the physical antenna as this lowers the noise introduced via the transmission medium.

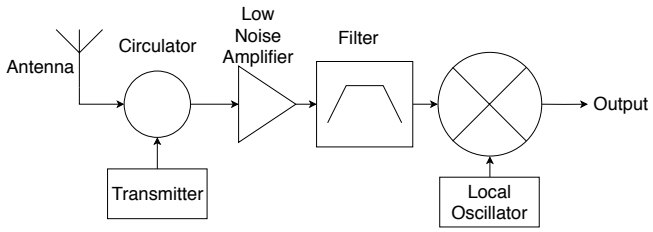

Figure A11: Receiver Diagram

R COSTING ANALYSIS AND RESEARCH

In order to estimate the total cost of the system, previously implemented systems that have a similar functionality can be compared. The first of these is the EISCAT Svalbard Radar Project [43, p. 670] which estimated the cost of the array was approximately R 432 million in 1990, and the yearly operating costs approximated R 40 million. This cost is indicative of the technology at the time and these costs will be greatly reduced with the use of newer efficient technology. The estimate for the entire solid-state amplifier implementation was estimated to be R 300 million, this includes the cooling, control systems, and transmitter modules. This is a high estimate as the cost of this will have been reduced over time.

The second comparable system is that of the AMISR (used by Leo Labs), which is estimated, once construction was completed to cost approximately \$52 million (R 750 million) for the concept development and implementation [41, p. 333-337]. The yearly operational cost for the system is estimated to be approximately \$3 million (R 43 million). This estimate is closer to the cost requirements for this design as the systems are constructed with a number of similarities for the components. The use of solid state amplifiers appears to be the best choice as the price of these components have decreased over the past two decades and their efficiency has increased. The Design document has a number of costing estimates for a solid-state amplifier implementation, however, this estimate was in 1990 [44, p. 37]. Table 8 illustrates the costing for an individual unit, this includes the antenna, transmitter and receiver components. The exchange rate is taken as R 14.40/\$. Based on average prices of antennas with similar characteristics [32–35, 45], the cost estimate for the antenna is chosen to be approximately R 10 000, which is a high estimate, however, this takes into consideration the requirements for the antenna to have a high tolerance, high power capability, low VSWR, and high efficiency. The communications unit is required to communicate with the CMM such that the antenna that it is connected to is operated in the required way. This system is housed within the antenna module as it should be shielded from the antenna and surrounding equipment. The estimate for the component is set at R 20 000. The control unit is responsible for communicating the information between the communication module and the electronics within the system, this system is costed at R 15 000.

This implies that the cost of the array, purely from the antenna element units is estimated to be approximately R 258.65 million. This estimate is close to that of the EISCAT implementation as it is within 20 % of their estimate for the antenna system. This costing does not take into consideration the price of the installation of the data center, roads, water supply, electricity supply, control rooms, land, etc. It is assumed that the cost of these contribute to twice the value of the array. This means that the total cost of the system can be estimated to approach R 775.95 million.

Table 8: Antenna Module Costing

Component	ID	Number	Unit Price (R)	Amount (R)
Antenna	N/A	1	10 000 000	10 000 000
Control Unit	N/A	1	15 000	15 000
Communication Unit	N/A	1	20 000	20 000
LNA	$ZHL-100-3W+$ [46]	1	10 008	10 008
Filter	$SXBP-640+$ [47]	2	258.48	516.96
Mixer	$TUF-R5SM+$ [48]	1	186.48	186.48
SMA Connectors	$35F-35M50+$ [49]	5	935.28	4676.4
Cables	$141-10SM+$ [50]	5	136.66	683.28
DC Blocker	$BLK-89-S+$ [51]	1	215.28	215.28
Oscillator	$Z0S-765+$ [52]	1	1727.28	1727.28
Circulator	$SKYFR-000736$ [53]	1	143.28	143.28
Total				63 146.96

S CODE LISTINGS

S1 Radar Calculations

The following code illustrates a number of calculations that are required to determine the orbital parameters of space debris. It also details the calculation of the parameters that are used for the antenna array and how it is used.

```
# Observable time or Dwell Time

import math
import numpy

speedOfLight = 3*10**(8)
minDistance = 160 * 10**(3)
maxDistance = 2000 * 10**(3)
earthRadius = 6378 * 10**(3)
centerFrequency = 610*10**(6)
gravitationalConstant = 6.67408 * 10 ** (-11)
earthMass = 5.972 * 10 ** (24)
boltzmannsConstant = 1.38064852*10**-(23)
standardTemp = 290
numElements = 4096

# Lambda
Lambda = speedOfLight / centerFrequency
print("Lambda: " + str(round(Lambda,4)) + " m")
# Tangential velocity
minObjectPeriod = 5280 # Seconds
maxObjectPeriod = 7620 # Seconds
# maxObjectSpeed = (2 * math.pi * (earthRadius+minDistance))/(
    ↪ minObjectPeriod)
maxObjectSpeed = math.sqrt((gravitationalConstant * earthMass)/(
    ↪ earthRadius+minDistance))
```

```
minObjectSpeed = math.sqrt((gravitationalConstant * earthMass)/(
    ↪ earthRadius+maxDistance))

# Maximum Angle (from zenith) (Max steering ability designed)
maxAngle = 30 * (math.pi / 180)



# Slant Distance
elevation = (math.pi)/2 - maxAngle
maxSlantDistance = earthRadius * (math.sqrt((((earthRadius +
    ↪ maxDistance)**2)/(earthRadius**2)) - (math.cos(elevation)**2 ))
    ↪  - math.sin(elevation)) # Taking in the max angle (from zenith)
    ↪  and max distance
minSlantDistance = earthRadius * (math.sqrt((((earthRadius +
    ↪ minDistance)**2)/(earthRadius**2)) - (math.cos(elevation)**2 ))
    ↪  - math.sin(elevation)) # Taking in the max angle (from zenith)
    ↪  and min distance
print("Maximum Slant Distance: " + str(round(maxSlantDistance/1000,4)
    ↪ ) + " km")

# Assuming a 120 degrees maximum field of view (60 degrees max angle)
maxSlantDistanceFOV = earthRadius * (math.sqrt((((earthRadius +
    ↪ maxDistance)**2)/(earthRadius**2)) - (math.cos((math.pi/2 )-(
    ↪ math.pi/3))**2 )) - math.sin((math.pi/2 )-(math.pi/3)))

# Path Loss of signal (return trip)
pathLoss = 2 * (Lambda/(4 * math.pi * maxSlantDistance))

# Observable Time of object within the FOV
maxObservableTime = (((earthRadius + maxDistance)**(3.0/2.0))/(math.
    ↪ sqrt(gravitationalConstant * earthMass)))*(math.pi - 2 *
    ↪ elevation - 2 * math.asin((earthRadius)/(earthRadius +
    ↪ maxDistance) * math.cos(elevation)))

# Angular Velocity
maxAngularVelocity = (maxObjectSpeed)/(minDistance)
minAngularVelocity = (minObjectSpeed)/(maxDistance)

# Apparent Angular Velocity
apparentAngularVelocity = (2 * maxAngle)/(maxObservableTime)

# Linear Velocity (measured from center of earth from system)
minLinearVelocity = apparentAngularVelocity * minDistance
maxLinearVelocity = apparentAngularVelocity * maxDistance

# Max doppler shift
dopplerFrequencyShift = 2*((maxLinearVelocity)/(speedOfLight))*
    ↪ centerFrequency
print("Maximum Doppler Shift: " + str(round(dopplerFrequencyShift,4))
    ↪  + " Hz")
```

```
# Minimum radar cross section of object (min diameter of 10 cm)
minObjectRadius = 5 * 10**(-2)
minRCS = math.pi * minObjectRadius**(2)
print("Radar Cross Section: " + str(round(minRCS,4)) + " m2")

# Signal Round trip times
minRoundTripTime = 2 * (minDistance/speedOfLight)
maxRoundTripTime = 2 * (maxSlantDistance/speedOfLight)
print("Maximum Rount Trip Time: " + str(round(maxRoundTripTime,4)) +
    ↪ " s")


# Pulse Width and Range Resolution Limits
maxBandwidth = 8 * 10**6
pulseWidthMin = 1/maxBandwidth
pulseWidthMax = minRoundTripTime
rangeResolutionMin = (speedOfLight * pulseWidthMin)/(2)

# Minimum Number of Pulses (based on HPBW of simulation)
HPBW = 0.785884 * (math.pi / 180)
elevationStationary = math.pi/2 - HPBW

maxObservableTimeStationary = (((earthRadius + minDistance)
    ↪ **(3.0/2.0))/(math.sqrt(gravitationalConstant * earthMass)))*(
    ↪ math.pi - 2 * elevationStationary - 2 * math.asin((earthRadius)
    ↪ /(earthRadius + minDistance) * math.cos(elevationStationary)))
print("Maximum amount of time object is in view (stationary beam): "
    ↪ + str(round(maxObservableTimeStationary,4)) + " s")
maxNumPulses = maxObservableTimeStationary/maxRoundTripTime
print("Maximum Number of Pulses with beam stationary: " + str(round(
    ↪ maxNumPulses,4)))
# Safe estimate pulse number
numPulses = 30

# Thermal Noise
noiseFiguredB = 2.5 # Measured in dB
noiseFigure = 10**(noiseFiguredB/10)

pulseWidth = 10 * 10**(-6)
bandwidth = 1 / pulseWidth
print("Bandwidth of the system: " + str(round(bandwidth/1000,4)) + "
    ↪ kHz")
SNRmindB = 10 #Measured in dB
SNRmin = 10**(SNRmindB/10)

gainPowerProduct = (SNRmin * (4 * (math.pi))**3 * maxSlantDistance**4
    ↪  * boltzmannsConstant * standardTemp * noiseFigure * bandwidth)
    ↪ /(Lambda**2 * minRCS * numPulses)

arrayGaindB = 41.0244
arrayGain = 10**(arrayGaindB/10)
```

```
maxPowerRequired = gainPowerProduct / ((arrayGain)**(2))
print("Maximum Power Required: " + str(round((maxPowerRequired
    ↪ /1000000),4)) + " MW")


dutyCycle = pulseWidth * (1/maxRoundTripTime)
print("Duty Cycle: " + str(round(dutyCycle,5)) + "%")
# print(dutyCycle)
averagePower = dutyCycle * maxPowerRequired
print("Average Power Required: " + str(round(averagePower/1000000,4))
    ↪  + " MW")

averagePowerPerElement = averagePower/numElements
maxPowerPerElement = maxPowerRequired/numElements

print("Average Power Per Element: " + str(round(
    ↪ averagePowerPerElement,4)) + " W")
print("Maximum Power Per Element: " + str(round(maxPowerPerElement
    ↪ /1000,4)) + " kW")


# Element Separation without Grating Lobes (assuming 30 degrees
    ↪ steering)
maxElementSpacing = (Lambda)/(1 + numpy.absolute(math.sin(maxAngle)))
print("Maximum Element Spacing: " + str(round(maxElementSpacing,4)) +
    ↪  " m")

# Range Resolution
rangeResolution = (speedOfLight * pulseWidth)/ 2
print("Range Resolution: " + str(round(rangeResolution/1000,2)) + "km
    ↪ ")
```

S2 Amplitude Tapering and Phasing

This portion of code is used to create the amplitude and phasing files that are used within FEKO to simulate the required antenna array parameters.

```
import math
import numpy
import matplotlib.pyplot as plt
import itertools

font = {'family' : 'normal',
        'size'   : 18}



speedOfLight = 3*10**8
minDistance = 160 * 10**3
maxDistance = 2000 * 10**3
earthRadius = 6378 * 10**3
```

```
centerFrequency = 610*10**6
gravitationalConstant = 6.67408 * 10 ** -11
earthMass = 5.972 * 10 ** 24
boltzmannsConstant = 1.38064852e-23

numRows = 64
numColumns = 64
# Lambda
Lambda = speedOfLight / centerFrequency

beta = (2 * math.pi)/(Lambda)


dx = Lambda/2
dy = Lambda/2

theta = 0
psi = 30

maxAmplitude = 1
minAmplitude = 0.5

w,h = numRows,numColumns
phaseMatrix = [[0 for x in range(w)] for y in range(h)]

d = Lambda/4
k = (2 * math.pi)/Lambda


f = open("phase.txt", "w+")
newline = ""
for x in range(0,numRows):
#     thetaSteer = x * ((math.pi)/4096 + k * d * math.cos(0)) * (-1)
    thetaSteer = x * (360 * dx * math.sin(math.radians(theta)))/(
        ↪ Lambda)
    for y in range(0,numColumns):
        psiSteer = y * (360 * dy * math.sin(math.radians(psi)))/(
            ↪ Lambda)
        # psiSteer = y * ((math.pi)/4096 - k * d * math.cos(0)) *
            ↪ (-1)
        totalSteer = thetaSteer + psiSteer
        phaseMatrix[x][y] = totalSteer
        outLine = newline + "1.0," + str(totalSteer)
        newline = "\n"
        f.write(outLine)

fig = plt.figure(figsize=(6, 3.2))
plt.rc('font', **font)
ax = fig.add_subplot(111)
ax.set_title('Heat Map Representing Phase Delay of Elements')
plt.imshow(phaseMatrix, cmap="Greys")
ax.set_aspect('equal')
```

```
cax = fig.add_axes([0.12, 0.1, 0.78, 0.8])
cax.get_xaxis().set_visible(False)
cax.get_yaxis().set_visible(False)
cax.patch.set_alpha(0)
cax.set_frame_on(False)
plt.colorbar(orientation='vertical', label="Phase Delay (degrees)")
plt.show()


#Amplitude
w,h = numRows,numColumns
amplitudeMatrix = [[0 for x in range(w)] for y in range(h)]

delta = numpy.linspace(0.5, 1.0, numRows/2)
deltaReverse = numpy.linspace(1.0, 0.5, numRows/2)
comb = numpy.concatenate((delta,deltaReverse))


for x in range(0,numRows):
    first = comb[x]
    for y in range(0,numColumns):
        second = comb[y]
        amplitudeMatrix[x][y] = (first + second)/2

print(amplitudeMatrix)

fig = plt.figure(figsize=(6, 3.2))

ax = fig.add_subplot(111)
ax.set_title('Heat Map Representing Amplitude Excitation of Elements'
    ↪ )
plt.imshow(amplitudeMatrix, cmap="Greys")
ax.set_aspect('equal')

cax = fig.add_axes([0.12, 0.1, 0.78, 0.8])
cax.get_xaxis().set_visible(False)
cax.get_yaxis().set_visible(False)
cax.patch.set_alpha(0)
cax.set_frame_on(False)
plt.colorbar(orientation='vertical', label="Percentage of Total Power
    ↪ ")
plt.show()

flattenedPhase = []
for x in phaseMatrix:
    for y in x:
        flattenedPhase.append(y)

flattenedAmplitude = []
for x in amplitudeMatrix:
    for y in x:
```

```
            flattenedAmplitude.append(y)

newline = ""
f = open("Amplitude.txt", "w+")
for x in range(0,numRows**2):
    outLine = newline + str(flattenedAmplitude[x])  + ",0.0"
    newline = "\n"
    f.write(outLine)

newline = ""
f = open("AmplitudePhase.txt", "w+")
for x in range(0,numRows**2):
    outLine = newline + str(flattenedAmplitude[x]) + "," + str(
        ↪ flattenedPhase[x])
    newline = "\n"
    f.write(outLine)
```

S3 Probability Analysis

This code listing provides the calculations that were used to generate the probability of detection and SNR while keeping the probability of false alarm at a specific set value.

```
numPulses = 1;
probabilityDetection = 0.3:0.01:1;
probabilityFalseAlarm = 10^(-1);
%10^(-8):10^(-1):10^(-1);

A = log(0.62/probabilityFalseAlarm);
B = log((probabilityDetection)./(1-probabilityDetection));

SNR1 = -5 .* log10(numPulses) + (6.2 + (4.54)./(sqrt(numPulses +
    ↪ 0.44))) .* log10(A + 0.12 .* A .* B + 1.7 .* B);

probabilityFalseAlarm = 10^(-2);
A = log(0.62/probabilityFalseAlarm);
SNR2 = -5 .* log10(numPulses) + (6.2 + (4.54)./(sqrt(numPulses +
    ↪ 0.44))) .* log10(A + 0.12 .* A .* B + 1.7 .* B);

probabilityFalseAlarm = 10^(-3);
A = log(0.62/probabilityFalseAlarm);
SNR3 = -5 .* log10(numPulses) + (6.2 + (4.54)./(sqrt(numPulses +
    ↪ 0.44))) .* log10(A + 0.12 .* A .* B + 1.7 .* B);

probabilityFalseAlarm = 10^(-4);
A = log(0.62/probabilityFalseAlarm);
SNR4 = -5 .* log10(numPulses) + (6.2 + (4.54)./(sqrt(numPulses +
    ↪ 0.44))) .* log10(A + 0.12 .* A .* B + 1.7 .* B);

probabilityFalseAlarm = 10^(-4);
A = log(0.62/probabilityFalseAlarm);
SNR5 = -5 .* log10(numPulses) + (6.2 + (4.54)./(sqrt(numPulses +
    ↪ 0.44))) .* log10(A + 0.12 .* A .* B + 1.7 .* B);
```

```
probabilityFalseAlarm = 10^(-5);
A = log(0.62/probabilityFalseAlarm);
SNR6 = -5 .* log10(numPulses) + (6.2 + (4.54)./(sqrt(numPulses +
    ↪ 0.44))) .* log10(A + 0.12 .* A .* B + 1.7 .* B);

hold on;
plot(real(probabilityDetection),SNR1,'k')
plot(real(probabilityDetection),SNR2,'k')
plot(abs(probabilityDetection),SNR3,'k')
plot(abs(probabilityDetection),SNR4,'k')
plot(abs(probabilityDetection),SNR5,'k')
plot(abs(probabilityDetection),SNR6,'k')
hold off;
```

S4 Simulation Documents

The simulation package, FEKO, is used throughout this design such that the proposed design can be analysed. The simulation files can be found in the following folder: https://goo.gl/d6mSqp

REFERENCES

[1] S. A. N. S. A. (SANSA). "SANSA — South African National Space Agency.", October 2018. URL https://goo.gl/LyoxBc.

[2] T. Valentic, J. Buonocore, M. Cousins, C. Heinselman, J. Jorgensen, J. Kelly, M. Malone, M. Nicolls, and A. V. Eyken. "AMISR the advanced modular incoherent scatter radar." In *2013 IEEE International Symposium on Phased Array Systems and Technology*, pp. 659–663. Oct 2013.

[3] J. Markkanen, M. Lehtinen, and M. Landgraf. "Real-time space debris monitoring with EISCAT." *Advances in Space Research*, vol. 35, no. 7, pp. 1197 – 1209, 2005. URL https://goo.gl/S3q4x3. Space Debris.

[4] S. A. S. K. Array. "Astronomy Geographic Land Act.", 2007. URL https://goo.gl/jij311.

[5] W. I. S. on Energy — WISE. "RADIOACTIVE SPACE DEBRIS: WHAT GOES UP, MUST COME DOWN.", June 2005. URL https://goo.gl/r5FDyH.

[6] RoHS. "RoHS Guide.", OCtober 2018. URL https://goo.gl/ZoiF92.

[7] S. H. F. Sun. "Extending the scanning angle of a phased array antenna by using a null-space medium.", OCtober 2018. URL https://goo.gl/GiKbyp.

[8] D. J. Kessler. "Collision frequency of artificial satellites: The creation of a debris belt." June 1978.

[9] A. S. Academy. "A GUIDE TO ORBITAL SPACE DEBRIS.", 2010. URL https://goo.gl/WpCRRp.

[10] U. Nations. "Space Debris Mitigation Guidelines of the Committee on the Peaceful Uses of Outer Space." January 2010. URL https://goo.gl/UPxRMv.

[11] F. Whipple. "Meteorites and space travel." 1947. URL https://goo.gl/yiGFqf.

[12] A. Parsonson. "RemoveDEBRIS Satellite Performs World's First In-Orbit Space Junk Capture.", September 2018. URL https://goo.gl/UqQYB5.

[13] C. on Space Debris. "Orbital Debris - A Technical Assessment." 1995.

[14] J. Chidgey. "Pragmatic 84: Space X.", December 2017. URL https://goo.gl/M6dEpK.

[15] C. V. E. Gill. "A New Approach for Enhanced Communication to LEO Satellites." April 2010.

[16] Z. Lu, M. Yao, and X. Deng. "An effective method for incoherent scattering radar's detecting ability evaluation." *Radio Science*, vol. 51, no. 6, pp. 852–857, June 2016.

[17] T. Hasenohr. "Initial Detection and Tracking of Objects in Low Earth Orbit." URL https:

//goo.gl/WctGfF.
[18] D. Agaba, M. Inggs, and D. O'Hagan. "SIMO radar design for small space debris detection in the LEO." In *2015 IEEE Radar Conference (RadarCon)*, pp. 0551–0554. May 2015.
[19] J. R. Snell. "Optimizing orbital debris monitoring with optical telescopes." September 2010.
[20] A. Patyuchenko, M. Younis, and G. Krieger. "Reflector-based digital beam-forming radar system for space debris detection." In *11-th INTERNATIONAL RADAR SYMPOSIUM*, pp. 1–4. June 2010.
[21] A. Morselli, P. D. Lizia, G. Bianchi, C. Bortolotti, S. Montebugnoli, G. Naldi, F. Perini, G. Pupillo, M. Roma, M. Schiaffino, A. Mattana, E. Salerno, A. Magro, K. Z. Adami, R. Armellin, A. L. Sergiusti, W. Villadei, F. Dolce, M. Reali, and J. Paoli. "A new high sensitivity radar sensor for space debris detection and accurate orbit determination." In *2015 IEEE Metrology for Aerospace (MetroAeroSpace)*, pp. 562–567. June 2015.
[22] J. G. Trujillo, S. Halté, M. S. Pérez, and P. Besso. "On the design of a planar phased array radar antenna architecture for space debris situational awareness." In *2013 7th European Conference on Antennas and Propagation (EuCAP)*, pp. 254–255. April 2013.
[23] U. Nations. "Technical Report on Space Debris." 1999.
[24] G. Curry. *Radar Essentials: A Concise Handbook for Radar Design and Performance Analysis*. Electromagnetics and Radar. Institution of Engineering and Technology, 2011. URL https://goo.gl/yiHxpz.
[25] T. Johnsen and K. E. Olsen. "Bi- and Multistatic Radar." https://goo.gl/J928KV.
[26] M. Richards, W. Holm, and J. Scheer. *Principles of Modern Radar: Basic Principles*. Electromagnetics and Radar. Institution of Engineering and Technology, 2010. URL https://goo.gl/az8neA.
[27] "Independent Communications Authority of South Africa.", October 2018. URL https://goo.gl/zXWsn1.
[28] "National Radio Frequency Plan 2018 (NRFP-18).", May 2018. URL https://goo.gl/MAzmL8.
[29] "Statistical Release.", 2016. URL https://goo.gl/c727Mq.
[30] P. Lehohla. "Census in brief.", 2011. URL https://goo.gl/Rx1fKd.
[31] R. of South Africa. "Government Gazette Act 21 of 2007: Astronomy Geographic Act.", 2007. URL https://goo.gl/5YFYcp.
[32] "Base antenna LEO eggbeater 70 cm 430-440 MHz RHCP.", October 2018. URL https://goo.gl/sjtqoS.
[33] "Turnstile crossed dipole NOAA receiving antenna for 137MHZ-139Mhz.", October 2018. URL https://goo.gl/vsghnE.
[34] "Turnstile crossed dipole antenna for 430 - 440Mhz (70cm).", October 2018. URL https://goo.gl/tJXSuF.
[35] "Turnstile crossed dipole Cubesat receiving antenna for 144Mhz-146Mhz (ISS,APRS,IGATE,SSTV).", October 2018. URL https://goo.gl/ECty3k.
[36] C. Balanis. *Antenna Theory: Analysis and Design*. No. v. 1 in Antenna Theory: Analysis and Design. John Wiley & Sons, 2005. URL https://goo.gl/RnbPim.
[37] "Vacant Land / Plot for sale in De Aar.", October 2018. URL https://goo.gl/mqNWAz.
[38] "3Ha Vacant Land For Sale in Keimoes.", October 2018. URL https://goo.gl/FZzUPU.
[39] "Vacant Land / Plot for Sale in Carnarvon.", January 2016. URL https://goo.gl/HJYnfA.
[40] S. SA. "INFRA SA Technical Response.", June 2013. URL https://goo.gl/aNX4DK.
[41] N. S. F. (NSF). "NSF Facilities FY 2006.", 2006. URL https://goo.gl/aCByD5.
[42] "Historical Rain Maps.", October 2018. URL https://goo.gl/m6n6sM.
[43] A. V. E. J. Rottger, U.G. Wannberg. "The EISCAT Scientific Association and the EISCAT Svalbard Radar Project." *EISCAT Scientific Association*, June 1995.
[44] P. C. R. W. GROUP. "THE EISCAT POLAR CAP RADAR - Report on the design specification for an incoherent scatter radar facility based on the archipelago of Svalbard.", November 1990. URL https://goo.gl/fdDceG.
[45] B. Warehouse. "RF Technologies AKG/1N." URL https://goo.gl/QyBU2D.

[46] M. Circuits. "Coaxial High Power Amplifier." URL https://goo.gl/k6pZQ4.
[47] M. Circuits. "Surface Mount Bandpass Filter." URL https://goo.gl/aQAfFZ.
[48] M. Circuits. "Surface Mount High Reliability Mixer." URL https://goo.gl/JGdwR8.
[49] M. Circuits. "Coaxial Adapter 3.5mm-F to 3.5mm-M." URL https://goo.gl/a85ftS.
[50] M. Circuits. "Coaxial Cable." URL https://goo.gl/5YKhJx.
[51] M. Circuits. "DC BLOCK / SMA-F / SMA-M /RoHS." URL https://goo.gl/Gu77Rj.
[52] M. Circuits. "VOLTAGE CONT OSC/SMA/BKT/ RoHS." URL https://goo.gl/YaJ3oz.
[53] RichardsonRFPD. "SKYFR-000736 Skyworks Solutions, Inc. Circulator/Isolator." URL https://goo.gl/rZXxdG.